Quantitative Analysis: The SEM/EDS Elemental Microanalysis k-ratio Procedure for Bulk Specimens, Step-by-Step

J. Goldstein et al., *Scanning Electron Microscopy and X-Ray Microanalysis*,
https://doi.org/10.1007/978-1-4939-6676-9_20

This chapter discusses the procedure used to perform a rigorous quantitative elemental microanalysis by SEM/EDS following the k-ratio/matrix correction protocol using the NIST DTSA-II software engine for bulk specimens. Bulk specimens have dimensions that are sufficiently large to contain the full range of the direct electron-excited X-ray production (typically 0.5–10 μm) as well as the range of secondary X-ray fluorescence induced by the propagation of the characteristic and continuum X-rays (typically 10–100 μm).

20.1 Requirements Imposed on the Specimen and Standards

The k-ratio/matrix correction protocol for the analysis of bulk specimens has two basic underlying assumptions:

1. The composition is homogeneous throughout the entire volume of the specimen in which primary characteristic X-rays are directly excited by the incident electron beam and in which secondary X-ray fluorescence is induced during the propagation of the primary characteristic and continuum X-rays. A compositionally heterogeneous specimen which does not satisfy this requirement cannot be analyzed by the conventional k-ratio/matrix correction protocol. Examples of such heterogeneous specimens include a horizontally layered specimen such as a thin film on a substrate or an inclusion with dimensions similar to the interaction volume embedded in a matrix. Such specimens must be analyzed with protocols that account for the effects of the particular specimen geometry.
2. The X-ray intensities measured on the location of interest on the specimen and on the standard(s) differ only because the compositions are different. No other factors modify the measured intensities. In particular, geometric effects that arise from physical surface defects, such as scratches, pits, and so on, can modify the interaction of the electron beam (electron backscattering, beam penetration) with the specimen and can alter the subsequent X-ray absorption path length to the detector compared to an ideal flat bulk specimen. This requirement places strict conditions on the surface condition of the specimen and standards. A highly polished, flat surface must be created following the appropriate metallographic preparation protocol for each particular material. The surface should be finished to a surface roughness below 100 nm root mean square (rms) with a typical final polish performed with 100-nm diamond, alumina, ceria or other polishing compound as appropriate. When the analysis involves measuring low energy photons below 1 keV (e.g., for the elements Be, B, C, N, O, and F), the surface finish should be better than 50 nm rms. The preparation protocol should utilize physical grinding and polishing. "Chemical polishing" should be avoided since chemical reactions may induce shallow, near-surface compositional changes that affect the very shallow region that is excited and sampled by the electron beam. Ion beam milling can be used to shape and finish the specimen, but it must be recognized that implantation of the primary ion and differential material removal caused by differences in the sputtering rates of the elements can modify the composition of a shallow surface layer.

20.2 Instrumentation Requirements

The basis of the k-ratio/matrix corrections protocol is measurement of the X-ray spectra of the specimen and standard (s) under identical conditions of beam energy, known electron dose (the product of beam current and EDS live-time, with accurate dead-time correction), EDS parameters (detector solid angle, time constant, calibration, and window efficiency), target orientation (tilt angle, ideally 0° tilt, i.e., beam perpendicular to the target surface), and EDS take-off angle (i.e., the detector elevation angle above the flat sample surface).

20.2.1 Choosing the EDS Parameters

Consistency in the choice of the EDS parameters is critical for establishing a robust analytical measurement environment, and this is especially important when archived standard spectra are used.

EDS Spectrum Channel Energy Width and Spectrum Energy Span

As shown in Fig. 20.1, when the energy axis is expanded sufficiently, the EDS spectrum is seen to be a histogram of energy channels of a specific width (e.g., 5 eV, 10 eV, 20 eV) and number (e.g., 1024, 2048, 4096). For accurate peak-fitting purposes, it is desirable to have an adequate number of channels spanning the characteristic X-ray peaks. Because the EDS resolution is a function of photon energy, low photon energy peaks below 1 keV are substantially narrower than higher energy peaks. A choice of 5 eV for the channel energy width will provide a sufficient number of channels to adequately span all of the peaks of analytical interest, including the peaks that occur below 1 keV. C K-$L_{2,3}$ is broadened in EDS to approximately 50 eV full width at half-maximum (FWHM), so a choice of 5-eV/channel will provide at least 10 channels to span the low photon energy peaks, which is important for accurate peak fitting. It is also desirable for the measured spectrum to span the full range of the excited X-ray energy, from an effective threshold of approximately 100 eV to the Duane–Hunt limit, which corresponds to the incident beam

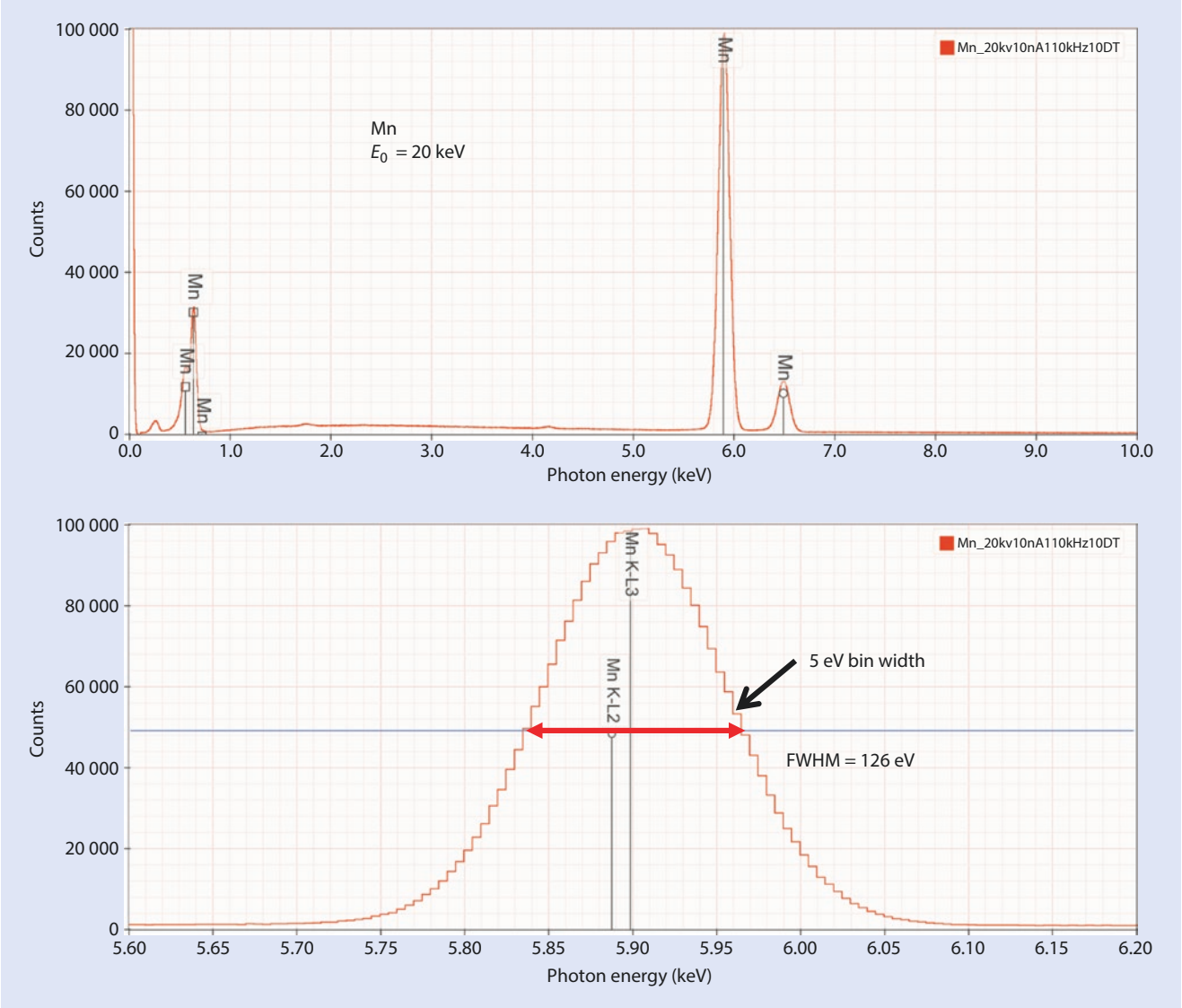

Fig. 20.1 SDD-EDS spectrum of Mn (E_0 = 20 keV)

energy, E_0. The energy span is given by the channel width multiplied by the number of channels. With a 5-eV channel width, a choice of 4096 channels will provide access to photon energies as high as 20.48 keV. For beam energy above 20 keV, the number of channels should be increased to retain the 5-eV channel width, or alternatively the channel width can be increased to 10 eV, but with the consequence that fewer channels will describe each characteristic peak.

EDS Time Constant (Resolution and Throughput)

The EDS is only capable of processing one photon at a time. The basic measurement cycle is the photoelectric absorption of the photon in the detector active volume, measurement of the charge deposited by scattering of the photoelectron to determine the photon energy, and incrementing the appropriate energy bin in the EDS histogram by one count. The EDS time constant (also known as the shaping time, the processing time, the maximum throughput, or other terms in different vendor EDS systems) effectively determines the amount of time spent on the measurement cycle. A short time constant enables more photons to be processed per unit of real (clock) time, but the trade-off of faster processing is poorer accuracy in assigning the photon energy. While the characteristic X-ray peak has a sharply defined energy, with a natural peak width of a few eV or less, the EDS measurement process inevitably substantially broadens the measured peak. For example, Mn K-$L_{2,3}$ has a natural width of approximately 7 eV (determined as the FWHM) but as displayed in the EDS histogram, the Mn K-$L_{2,3}$ peak is broadened to 122–150 eV

FWHM or more, depending on the choice of time constant. For the particular silicon drift detector (SDD)-EDS and time constant shown in Fig. 20.1, the broadened EDS peak has a FWHM = 126 eV. The peak width increases (i.e., resolution becomes poorer) as the time constant decreases. The shortest time constant, which gives the highest throughput but the broadest peaks (poorest resolution), is typically chosen for analysis situations where it is important to maximize the total number of X-ray counts per unit of clock (real) time, such as elemental X-ray mapping. For quantitative analysis, better peak resolution is desirable, and thus a longer time constant should be chosen. Whichever time constant strategy is selected, it is important for standards-based quantitative analysis that this same time constant be used for all measurements of unknowns and standards, especially if archived standards are used.

EDS Calibration

Assigning the proper energy bin for a photon measurement depends on the EDS being calibrated. The vendor for a particular EDS system will have a recommended calibration procedure that should be followed on a regular basis as part of establishing a quality measurement environment, with full documentation of the measurements to establish the on-going calibration record. A typical calibration strategy is to choose a material such as Cu that provides (with $E_0 \geq 15$ keV) strongly excited peaks in the low photon energy range (Cu $L_3M_5 = 0.93$ keV) and the high photon energy range (Cu K-$L_{2,3} = 8.04$ keV). Alternatively, some EDS systems that provide a "zero energy reference" signal will use this value with a single high photon energy peak such as Cu K-$L_{2,3}$ or Mn K-$L_{2,3}$ to perform calibration. A good quality assurance practice is to begin each measurement campaign by measuring a spectrum of Cu (or another element, e.g., Mn, Ni, etc., or a compound, e.g., CuS, FeS_2, etc.) under the user-defined conditions. This Cu spectrum can be compared to the Cu spectrum that is stored in the archive of standards to confirm that the current measurement conditions are identical to those used to create the archive. This starting Cu spectrum should always be saved as part of the quality assurance plan.

EDS Solid Angle

The solid angle of collection, Ω, is given by

$$\Omega = A / r^2 \qquad (20.1)$$

where A is the active area of the detector and r is the distance from the X-ray source on the specimen to the detector. Some EDS systems are mounted on a retractable arm that enables the analyst to choose the value of r. A consistent and reproducible choice must be made for r since this value has such a strong impact on Ω and thus on the number of photons detected per unit of dose.

20.2.2 Choosing the Beam Energy, E_0

The choice of beam energy depends on the particular aspects of the analysis that the analyst wishes to optimize. As a starting point, a useful general analysis strategy is to optimize the excitation of photon energies up to 12 keV by choosing an incident beam energy of 20 keV, which provides sufficient overvoltage ($E_0/E_c > 1.5$) for K-shell (to Br) and L-shell (elements to Bi) for reasonable excitation. The characteristic peaks of X-ray families that occur in the photon energy range from 4 keV to 12 keV are generally sufficiently separated in energy to be resolved by EDS. When it is important to measure those elements whose characteristic peaks occur below 4 keV, and especially for the low atomic number elements Be, B, C, N, O and F, for which the characteristic peaks occur below 1 keV and suffer high absorption, then analysis with lower beam energy, 10 keV or lower, will be necessary to optimize the results.

20.2.3 Measuring the Beam Current

The SEM should be equipped for beam current measurement, ideally with an in-column Faraday cup which can be selected periodically during the analysis procedure to determine the beam current. As an alternative, a picoammeter can be installed between the electrically isolated specimen stage and the electrical ground to measure the absorbed (specimen) current that must flow to ground to avoid specimen charging. The specimen current is the difference between the beam current and the loss of charge due to BSE and SE emission, both of which vary with composition. To measure the true beam current, BSE and SE emission must be recaptured, which is accomplished by placing the beam within a Faraday cup, which is constructed as a blind hole in a conducting material (e.g., metal or carbon) covered with a small entrance aperture (e.g., an electron microscope aperture of 50 µm diameter or less). This Faraday cup is then placed at a suitable location on the electrically isolated specimen stage. By locating the beam in the center of the Faraday cup aperture opening, the primary beam electrons as well as all BSEs and SEs generated at the inner surfaces are collected with very little loss through the small aperture, so that the current flowing to the electrical ground is the total incident beam current.

20.2.4 Choosing the Beam Current

After the analyst has chosen the EDS time constant, the detector solid angle (for a retractable detector), and the beam energy, the beam current should be chosen so as to give a reasonable detector throughput, as expressed by the system dead-time. Figure 20.2 shows the relationship between the input count rate (ICR) of X-rays that arrive at the detector and the output count rate (OCR) of photons that are actually stored in the measured spectrum. The OCR initially rises linearly with the ICR, but as photons arrive at a progressively greater rate at the detector, photon coincidence begins to occur and the anti-coincidence function begins to reject these coincidence events, reducing the OCR. Eventually a maximum OCR value is reached beyond which the OCR decreases with increasing ICR, eventually falling to zero ("paralyzable dead-time"). A useful measure of the activity state of the EDS detector is the system "dead-time" which is defined as

$$\text{Dead-time}(\%) = \left[(\text{ICR} - \text{OCR}) / \text{ICR}\right] * 100 \qquad (20.2)$$

A classic strategy with the low throughput Si(Li)-EDS is to select a beam current on a highly excited pure element such as Al or Si that produces a dead-time of 30 % or less. With SDD-EDS, a more conservative counting strategy is suggested, such that the beam current is chosen so that the dead-time on the most highly excited standard of interest, for example, Al or Si, is less than 10 %. Despite the operation of the anti-coincidence function, SDD-EDS systems typically show evidence of coincidence peaks above a dead-time of 10 % from highly excited parent peaks, as illustrated in Fig. 20.3, which shows the in-growth of an extensive set of coincidence peaks from several parent peaks. If it is important to measure low intensity X-ray peaks that correspond to minor or trace constituents that occur in spectral regions affected by coincidence peaks, then choosing the low dead-time to minimize coincidence will be an important issue in selecting the general analytical conditions. If there is no interest in measuring X-ray peaks of possible constituents that occur in the region of coincidence peaks, then these regions can be ignored and a counting strategy that involves higher dead-time operation can be used.

Once the analytical conditions (EDS time constant, solid angle, beam energy, and beam current appropriate to the complete suite of standards) have been chosen, these conditions should be used for all standards and unknowns to achieve the basic measurement consistency required for the k-ratio/matrix corrections protocol.

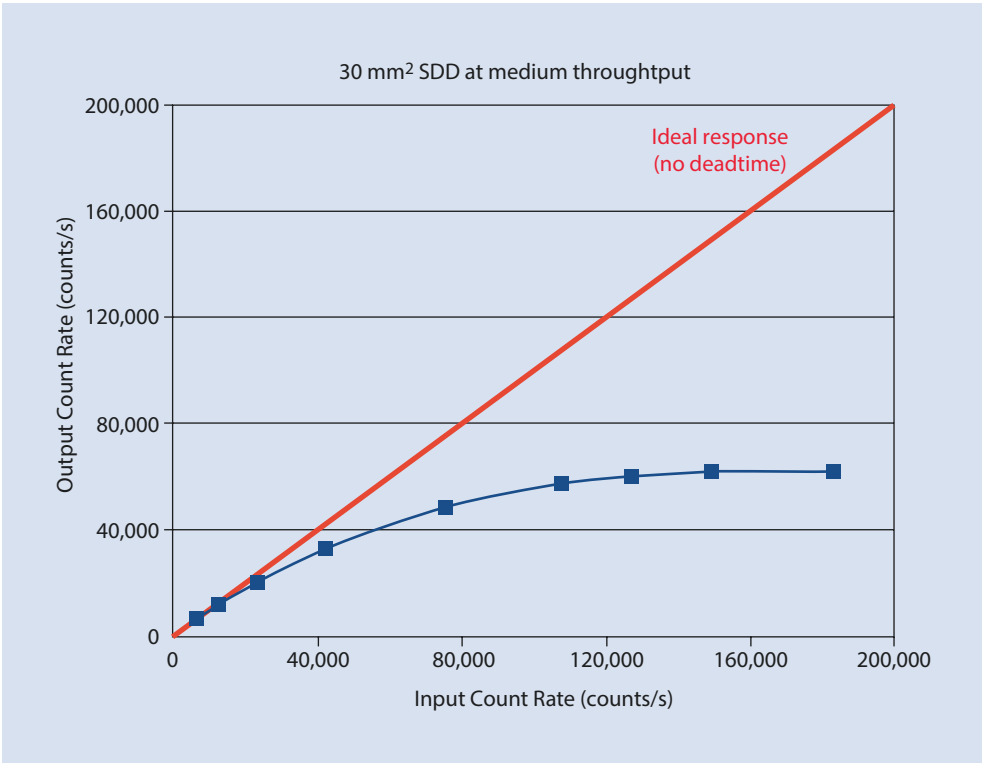

Fig. 20.2 Output count rate (OCR) vs. input count rate for an SDD-EDS array of four 10-mm² detectors

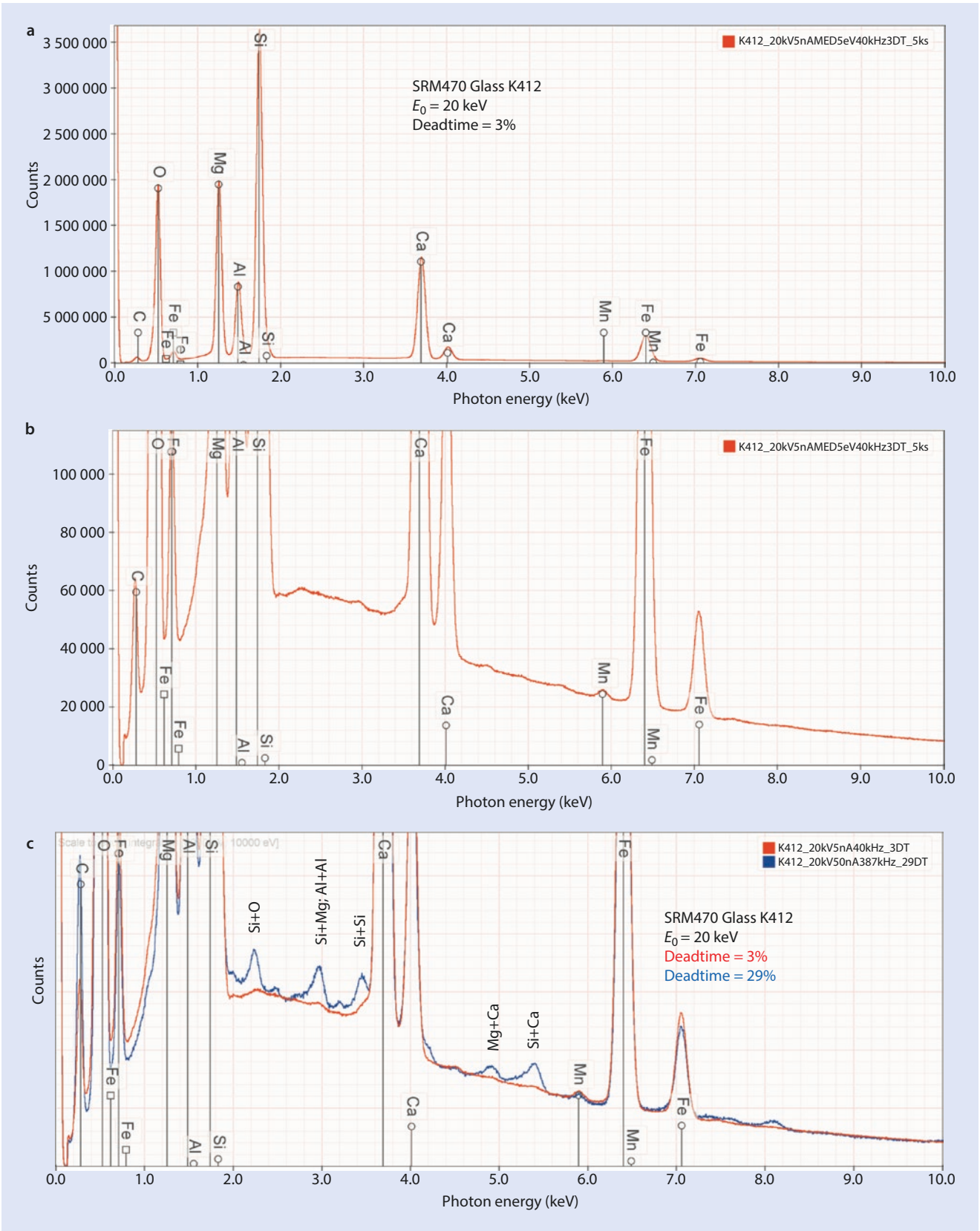

Fig. 20.3 SDD-EDS spectra of NIST SRM (glass K412, E_0 = 20 keV: **a**, **b** at 3 % dead-time (*red*); **c** 3 % (*red*) and 29 % dead-time (*blue*), showing in-growth of coincidence peaks

20.3 Examples of the k-ratio/Matrix Correction Protocol with DTSA II (Newbury and Ritchie 2015b)

20.3.1 Analysis of Major Constituents (C > 0.1 Mass Fraction) with Well-Resolved Peaks

The EDS spectra of the minerals pyrite (FeS_2) and troilite (FeS) measured at $E_0 = 20$ keV with a dead-time of ~ 10 % are shown in Fig. 20.4 and feature well separated peaks for the Fe K- and L- families and the S K-family. These spectra were analyzed with Fe and CuS serving both as peak-fitting references and as standards. CuS is chosen for the S reference and standard rather than elemental S since CuS is stable under electron bombardment while elemental S is not stable. The spectrum for FeS and the residual spectrum after peak-fitting are also shown in Fig. 20.4. The results for seven replicate analyses are listed in Table 20.1 (FeS) and Table 20.2 (FeS_2) along with the ZAF correction factors and the components of the error budget. In this analysis and the analyses reported below, the relative deviation from the expected value (RDEV) (also referred to as "relative error") is calculated with the "expected" value taken as the stoichiometric formula value or the value obtained from an "absolute" analytical method, just as in gravimetric analysis:

$$\mathrm{RDEV} = \left[\frac{(\text{Analyzed value} - \text{expected value})}{\text{expected value}}\right] \times 100\% \qquad (20.3)$$

Optimizing Analysis Strategy

The DTSA II analysis report includes for each analyzed element the ZAF factors and the estimated uncertainties in these factors as well as uncertainties due to the counting statistics associated with the measurements of the unknown and of the standard (Ritchie and Newbury 2012). Careful examination of these factors can be used to refine the analytical strategy to optimize the measurement. Reducing the uncertainty due to the counting statistics requires increasing the dose. The absorption factor A is strongly influenced by the

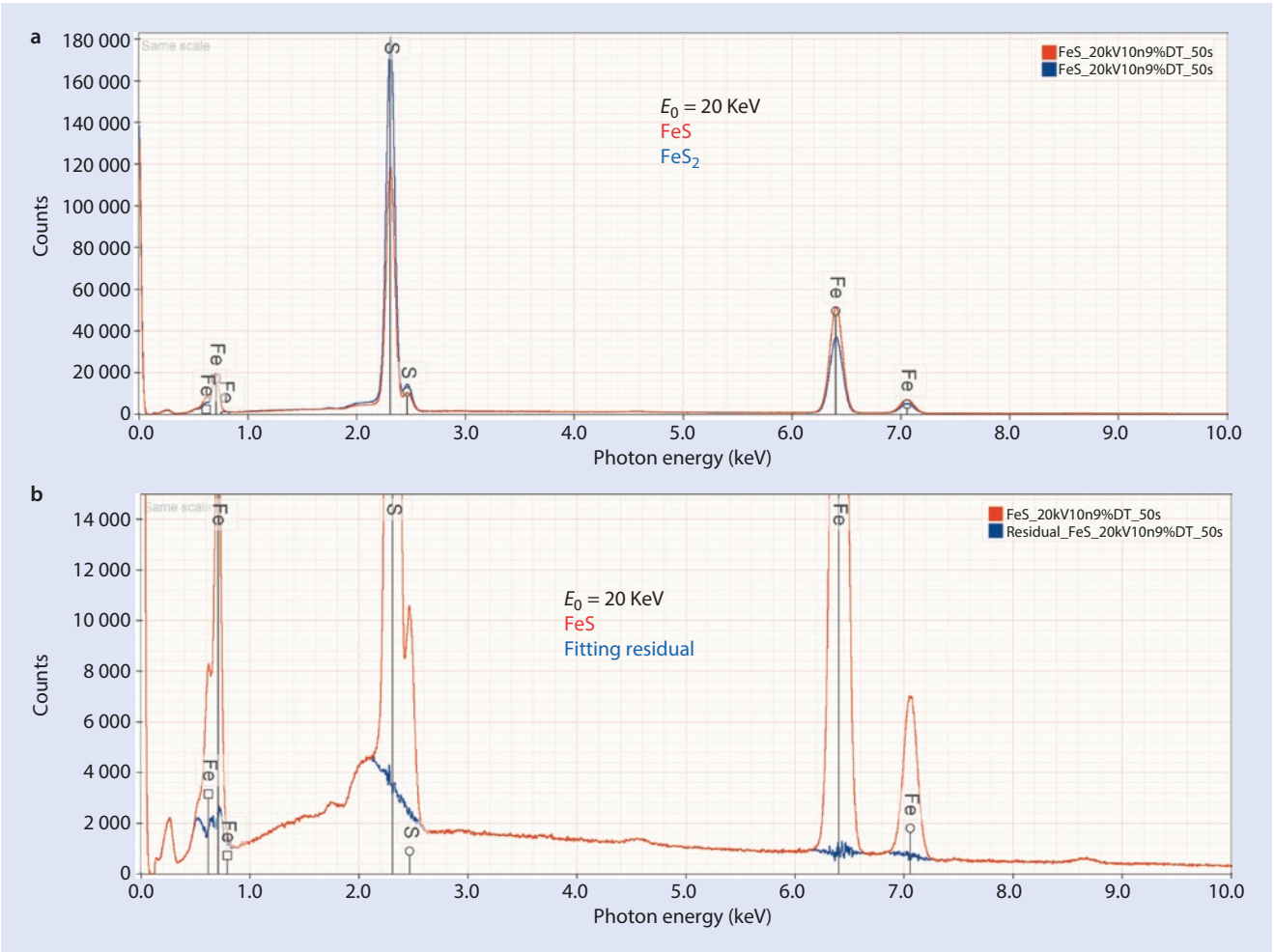

Fig. 20.4 **a** SDD-EDS spectra of Pyrite (FeS_2) (*blue*) and meteoritic Troilite (FeS (*red*) at $E_0 = 20$ keV. **b** NIST DTSA-II analysis of FeS using Fe and CuS as peak-fitting references and as standards. The original spectrum (*red*) and the residual spectrum after peak-fitting (*blue*) are shown

Table 20.1 Analysis of FeS (meteoritic troilite) at $E_0 = 20$ keV with CuS and Fe as fitting references and standards Integrated spectrum count, 0.1–20 keV = 7,048,000; uncertainties expressed in mass fraction. Analysis performed with Fe K-$L_{2,3}$ and S K-$L_{2,3}$

	S	Fe
C_{av} (atom frac)	0.5052	0.4948
Z-correction	0.977	0.95
A-correction	1.118	0.983
F-correction	1.003	1
σ (7 replicates)	0.00075	0.00075
σ_{Rel} (%)	0.15 %	0.15 %
RDEV (%)	1.00 %	−1.00 %
C (mass frac, single analysis)	0.3699	0.6305
Counting error, std	0.00020	0.0003
Counting error, unk	0.00020	0.0007
A-factor error	0.0017	0.0002
Z-factor error	2.20×10^{5}	4.10×10^{-6}
Combined errors	0.0017	0.0008

Table 20.2 Analysis of FeS_2 (pyrite) at $E_0 = 20$ keV with CuS and Fe as fitting references and standards Integrated spectrum count, 0.1.–20 keV = 7,765,000; uncertainties expressed in mass fraction. Analysis performed with Fe K-$L_{2,3}$ and S K-$L_{2,3}$

	S	Fe
C_{av} (atom frac)	0.6726	0.3274
Z-correction	0.957	0.928
A-correction	1.181	0.975
F-correction	1.003	1
σ (7 replicates)	0.000314	0.000314
σ_{Rel} (%)	0.05 %	0.10 %
RDEV (%)	0.88 %	−1.80 %
C (mass frac, single analysis)	0.5485	0.4657
Counting error, std	0.0003	0.0002
Counting error, unk	0.0003	0.0006
A-factor error	0.0023	0.0002
Z-factor error	3.30×10^{-5}	2.90×10^{-6}
Combined errors	0.0023	0.0007

Table 20.3 Analysis of FeS at $E_0 = 10$ keV with CuS and Fe as fitting references and standards Integrated spectrum count, 0.1–10 keV = 5,630,000; uncertainties expressed in mass fraction. Analysis performed with Fe K-$L_{2,3}$ and S K-$L_{2,3}$

	S	Fe
C_{av} (atom frac)	0.503	0.497
Z-correction	0.973	0.937
A-correction	1.041	0.997
F-correction	1.001	1
σ (7 replicates)	0.00056	0.00056
σ_{Rel} (%)	0.11 %	0.11 %
RDEV (%)	0.59 %	−0.59 %
C (mass frac, single analysis)	0.3627	0.6257
Counting error, std	0.0002	0.0008
Counting error, unk	0.0003	0.0018
A-factor error	0.0006	4.10E-05
Z-factor error	2.20×10^{-5}	1.30×10^{-6}
Combined errors	0.0007	0.0019

Table 20.4 Analysis of FeS_2 at $E_0 = 10$ keV with CuS and Fe as fitting references and standards Integrated spectrum count, 0.1–10 keV = 6,253,000); uncertainties expressed in mass fraction. Analysis performed with Fe K-$L_{2,3}$ and S K-$L_{2,3}$

	S	Fe
C_{av} (atom frac)	0.671	0.329
Z-correction	0.95	0.91
A-correction	1.061	0.995
F-correction	1.001	1
σ (7 replicates)	0.0007	0.0007
σ_{Rel} (%)	0.11 %	0.21 %
RDEV (%)	0.65 %	−1.30 %
C (mass frac, single analysis)	0.537	0.4618
Counting error, std	0.0003	0.0006
Counting error, unk	0.0003	0.0016
A-factor error	0.0008	4.30E-05
Z-factor error	3.20×10^{-5}	9.60×10^{-7}
Combined errors	0.0009	0.0017

choice of beam energy. If the beam energy can be decreased, considering also the constraints imposed by having sufficient overvoltage for all elements to be analyzed, the absorption correction factor and its uncertainty can also be reduced. For the Fe-S examples, lowering the beam energy from 20 to 10 keV gives the results shown in Tables 20.3 and 20.4. The absorption factor A from is reduced from 1.118 to 1.04 for S in FeS and from 1.18 to 1.06 for S in FeS_2, and the relative errors are also reduced slightly, from 1 to 0.59 % for S in FeS and from 0.88 to 0.65 % for S in FeS_2.

20.3.2 Analysis of Major Constituents (C > 0.1 Mass Fraction) with Severely Overlapping Peaks

PbS

The throughput and the peak stability (calibration and resolution) of SDD-EDS spectrometry enable collection of high count, high quality spectra (>5 million counts) within modest measurement time, 100 s or less. High count spectra enable measurements of minor and trace constituents with high precision. High counts and stable peak structures are critical for successful peak intensity measurements by peak-fitting methods, which is especially important for situations where two or more peaks are so close in photon energy that the EDS resolution function convolves the peaks into mutual interference. Despite extreme peak interference, quantitative X-ray microanalysis can be achieved with RDEV values of 5 % relative or less (Newbury and Ritchie 2015a).

PbS (galena) represents a challenging analysis situation for EDS because of the severe interference between the S K-L_2 (2.307 keV) and Pb M_5-$N_{6,7}$ (2.343 keV), which are separated by 36 eV, as shown in Fig. 20.5. Analysis of PbS with DTSA II using CuS and PbSe as peak-fitting references and as standards yields the results in Table 20.5. Despite the severe peak interference, the relative error based on the formula stoichiometry is only ±1.2 % for S and Pb.

Note that an alternative analytical approach would be to select the beam energy such that $E_0 \geq 20$ keV so that the Pb L-family is excited ($L_{III} = 13.04$ keV). With this choice of excitation, the Pb L_3-$M_{4,5}$ peak at 10.55 keV, which does not suffer interference, could be chosen to measure Pb. Of course, the S K still must be deconvoluted from the interference from the Pb M-family since there is no alternate peak to measure for S.

MoS_2

MoS_2 represents an even greater analytical challenge because the peaks that must be used for analysis, S K-L_2 (2.307 keV) and Mo L_3-$M_{4,5}$ (2.293 keV), are separated by only 14 eV, as shown in Fig. 20.6. Analysis of MoS_2 with DTSA II using CuS and Mo as peak-fitting references and as standards yields the results in Table 20.6. Despite the severe peak interference, the relative error based on the formula stoichiometry is only −0.34 % for S and 0.7 % for Mo.

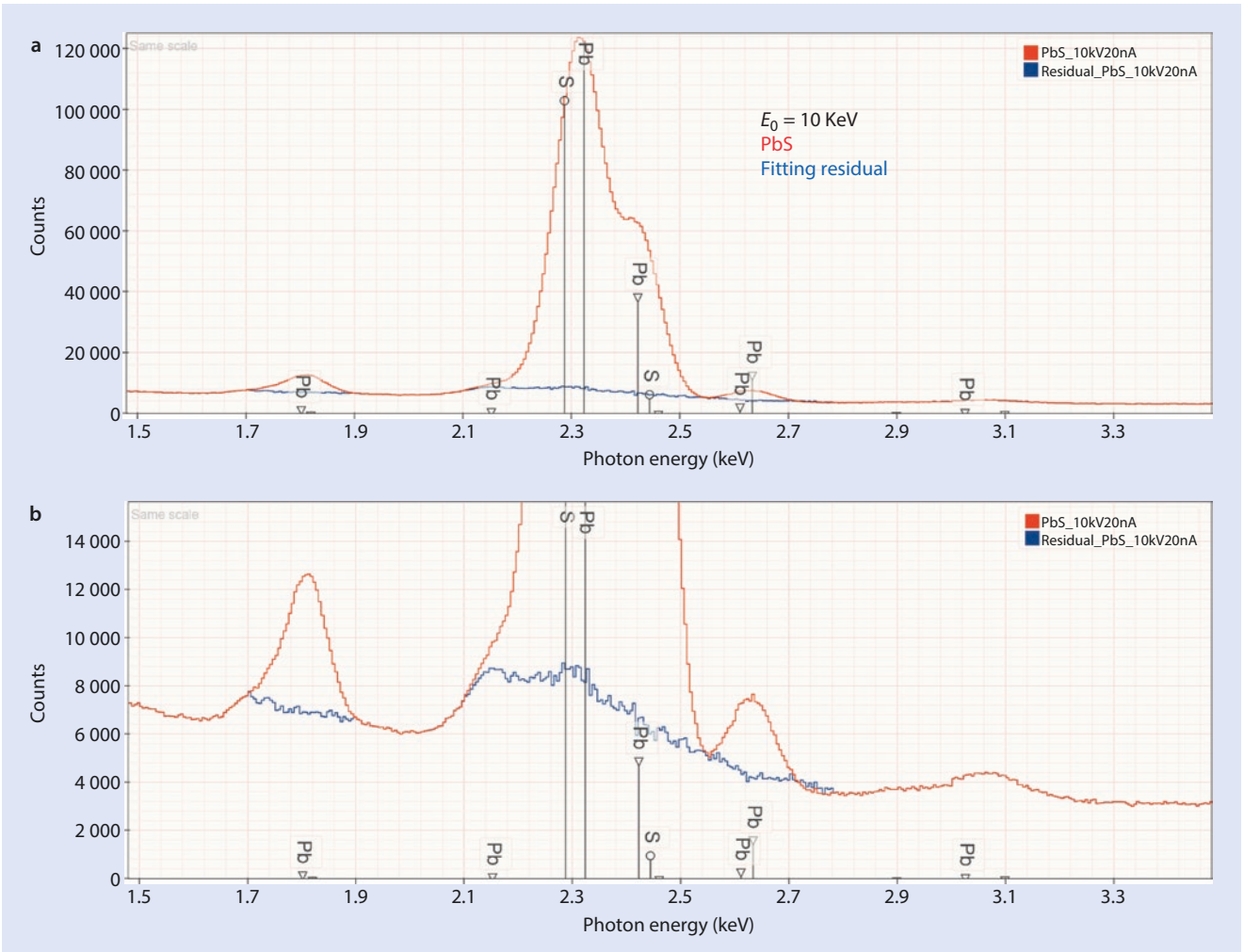

Fig. 20.5 **a** SDD-EDS spectrum of PbS (*red*) and residual (*blue*) after DTSA II analysis using CuS and PbSe as fitting references and standards. **b** Expanded view

Table 20.5 Analysis of PbS at $E_0 = 10$ keV with CuS and PbSe as fitting references and standards; Integrated spectrum count, 0.1–10 keV = 5,482,000; uncertainties expressed in mass fraction. Analysis performed with Pb M_5-$N_{6,7}$ and S K-$L_{2,3}$

	S	Pb
C_{av} (atom frac)	0.4938	0.5062
Z-correction	1.31	0.983
A-correction	1.028	1.056
F-correction	1	1
σ (7 replicates)	0.000953	0.000953
σ_{Rel} (%)	0.19 %	0.19 %
RDEV (%)	−1.20 %	1.2
C (mass frac, single analysis)	0.1306	0.8651
Counting error, std	0.0001	0.0009
Counting error, unk	0.0003	0.001
A-factor error	0.0002	0.0017
Z-factor error	1.50×10^{-5}	0.0001
Combined errors	0.0004	0.0022

20.3.3 Analysis of a Minor Constituent with Peak Overlap From a Major Constituent

The problem of accurately recovering peak intensities when overlaps occur is exacerbated when the concentration ratio of the elements producing the overlapping peaks is large, for example, a major constituent (C > 0.1 mass fraction) interfering with a minor ($0.01 \leq C \leq 0.1$) constituent. The high throughput (>100 kHz output count rate) of SDD-EDS enables collection of high count EDS spectra in modest collection time (e.g., 10 million counts in 100 s). Moreover, the high throughput of SDD-EDS is achieved with stability in both the peak position (i.e., calibration) and the peak shape (i.e., resolution) across the entire input count rate range. In simultaneous WDS-EDS measurements, this SDD-EDS performance been demonstrated to the spectrum measurement capabilities necessary for robust MLLS peak-fitting to achieve accurate measurement of the interfering peak intensities equal to that of WDS on the spectroscopically resolved peaks (Ritchie et al. 2012).

20.3.4 Ba-Ti Interference in $BaTiSi_3O_9$

$BaTiSi_3O_9$ (benitoite) provides an example of severe interference between two constituents of identical atomic concentration but with a mass concentration ratio of Ba/Ti = 2.9—Ti K-$L_{2,3}$ (4.510 keV) and Ba L3-$M_{4,5}$ (4.466 keV)—which are separated by 44 eV, as shown in Fig. 20.7. DTSA II analysis of benitoite with Ti and sanbornite ($BaSi_2O_5$) as fitting references and standards is given in Table 20.7. Note that in this analysis, O has been directly analyzed with the k-ratio/matrix corrections protocol and not by the method of assumed stoichiometry. The analytical results are seen to closely match the stoichiometry of the ideal mineral formula.

20.3.5 Ba-Ti Interference: Major/Minor Constituent Interference in K2496 Microanalysis Glass

NIST microanalysis research material K2496 glass contains these same elements, but with Ba as a major constituent ($C = 0.4299$ mass fraction) and Ti as a minor constituent ($C = 0.01799$ mass fraction), giving an elemental ratio of Ba/Ti = 23.9. Figure 20.8a shows the SDD-EDS spectrum and residual after peak fitting, and Table 20.8 contains the results of the analysis. Despite the severe overlap and the large elemental ratio, the concentration for Ti is measured with reasonable accuracy. A reasonable question that the analyst might ask is, If it was not known that the Ti was present, could it be detected? Figure 20.8b shows the fitting residual for an analysis protocol in which Ti was not fit. The peaks for Ti K-$L_{2,3}$ and Ti K-M_3 are revealed in the residual spectrum.

20.4 The Need for an Iterative Qualitative and Quantitative Analysis Strategy

The analysis of NIST glass K2496 demonstrates that rigorous analysis requires an iterative qualitative analysis–quantitative analysis approach. When analyzing an unknown material, it is likely that some constituents at the minor and trace level will not be obvious when the first qualitative analysis is performed due to peak interference from constituents at higher concentrations. An alternating qualitative–quantitative analytical strategy is required to discover possibly hidden minor and trace constituents. In the initial qualitative analysis, the EDS spectrum is evaluated to identify the major and minor elemental constituents whose peaks are readily identifiable. The k-ratio/matrix correction protocol is then applied with appropriate choices for elemental peak-fitting references and for standards, and the "residual" spectrum is constructed that contains the intensity remaining after the fitted peaks have been subtracted. If all constituents have been accounted for, this residual spectrum should only consist of the continuum background and possibly also artifact peaks such as escape and coincidence peaks. However, because of the relative poor energy resolution of EDS, the analyst must perform a second qualitative analysis of the residual spectrum for the presence of previously unrecognized peaks that are associated with constituents that suffer interference from the higher intensity peaks. If such peaks are discovered and assigned to an element(s) not previously recognized, the quantitative analysis must then be repeated with this element(s) included in the peak-fitting and

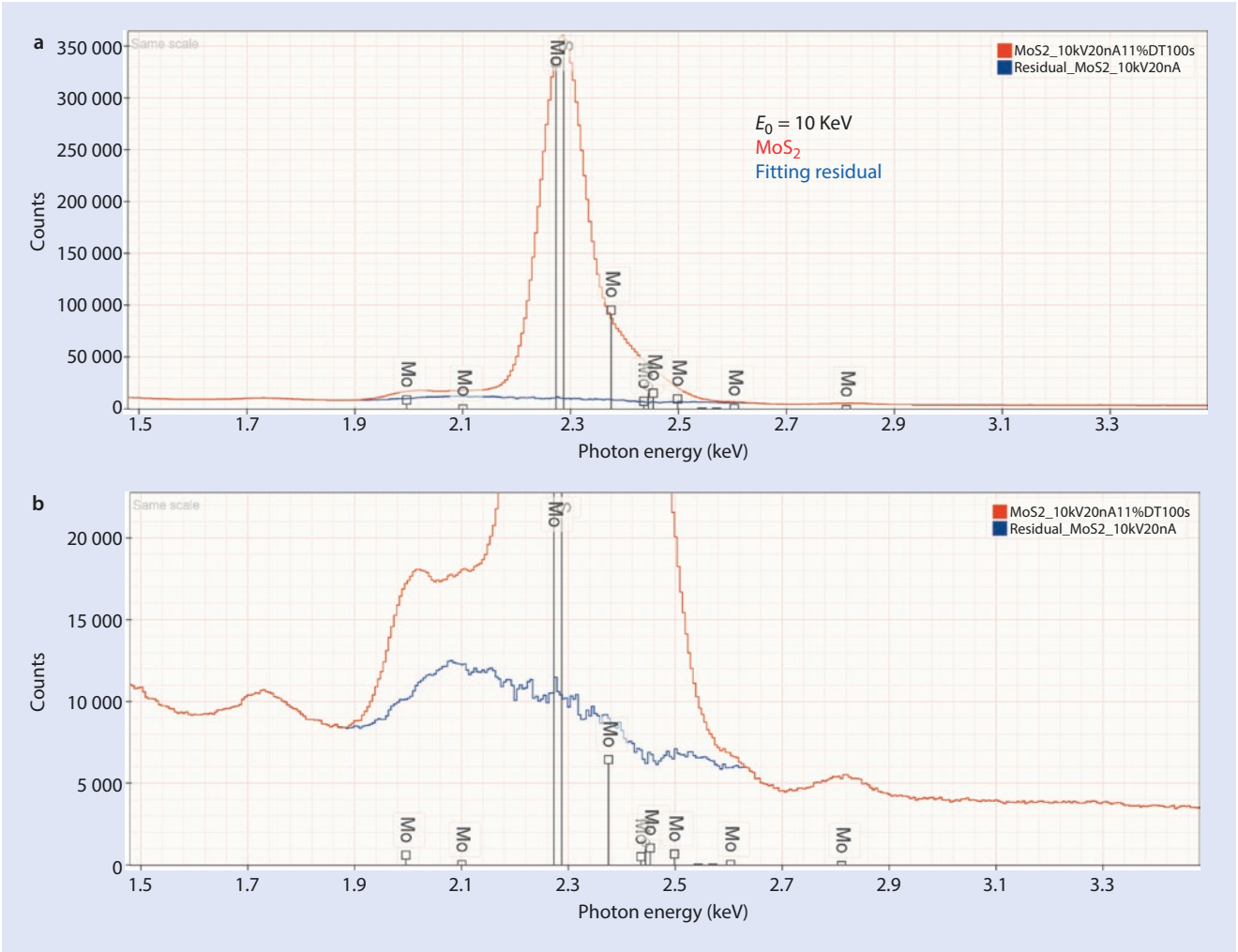

Fig. 20.6 **a** SDD-EDS spectrum of MoS_2 (*red*) at $E_0 = 10$ keV (7,326,000 counts) and residual (*blue*) after DTSA II analysis using CuS and Mo as fitting references and standards. **b** Expanded view

Table 20.6 Analysis of MoS_2 at $E_0 = 10$ keV with CuS and Mo as fitting references and standards; integrated spectrum count, 0.1–10 keV = 7,326,000; uncertainties expressed in mass fraction. Analysis performed with Mo $L_{2,3}$-$M_{4,5}$ and S K-$L_{2,3}$

	S	Mo
C_{av} (atom frac)	0.6644	0.3356
Z-correction	1.039	0.884
A-correction	1.083	1.024
F-correction	1	1
σ (7 replicates)	0.0022	0.0022
σ_{Rel} (%)	0.33 %	0.66 %
RDEV (%)	−0.34 %	0.70 %
C (mass frac, single analysis)	0.3972	0.6046
Counting error, std	0.0003	0.0003
Counting error, unk	0.0006	0.0014
A-factor error	0.0006	0.0006
Z-factor error	2.80×10^{-5}	4.40×10^{-5}
Combined errors	0.0008	0.0015

quantification suite of elements. A third iteration may be necessary to recover constituents present at the trace level near the limits of detection.

20.4.1 Analysis of a Complex Metal Alloy, IN100

IN100 is a nickel-based superalloy which produces the EDS spectrum shown in Fig. 20.9. In the first qualitative analysis, characteristic X-ray peaks were identified for Al K; the Ti K-family; the Cr, Co, and Ni K- and L- families; and Mo L-family. Analysis with the k-ratio/matrix correction protocol using pure elements as peak-fitting references and as standards gave the results shown in Table 20.9, with the analytical total slightly below unity. Close inspection of the residual spectrum in Fig. 20.9 showed an anomaly at the energy of Ti K-$M_{4,5}$ (4.931 keV)) which closely corresponds to the energy of V K-$L_{2,3}$ (4.952 keV) with a separation of 21 eV. When V was included in the suite of fitted elements, the anomaly in the residual spectrum was eliminated, as shown in Fig. 20.10, and a minor V constituent was recovered in the

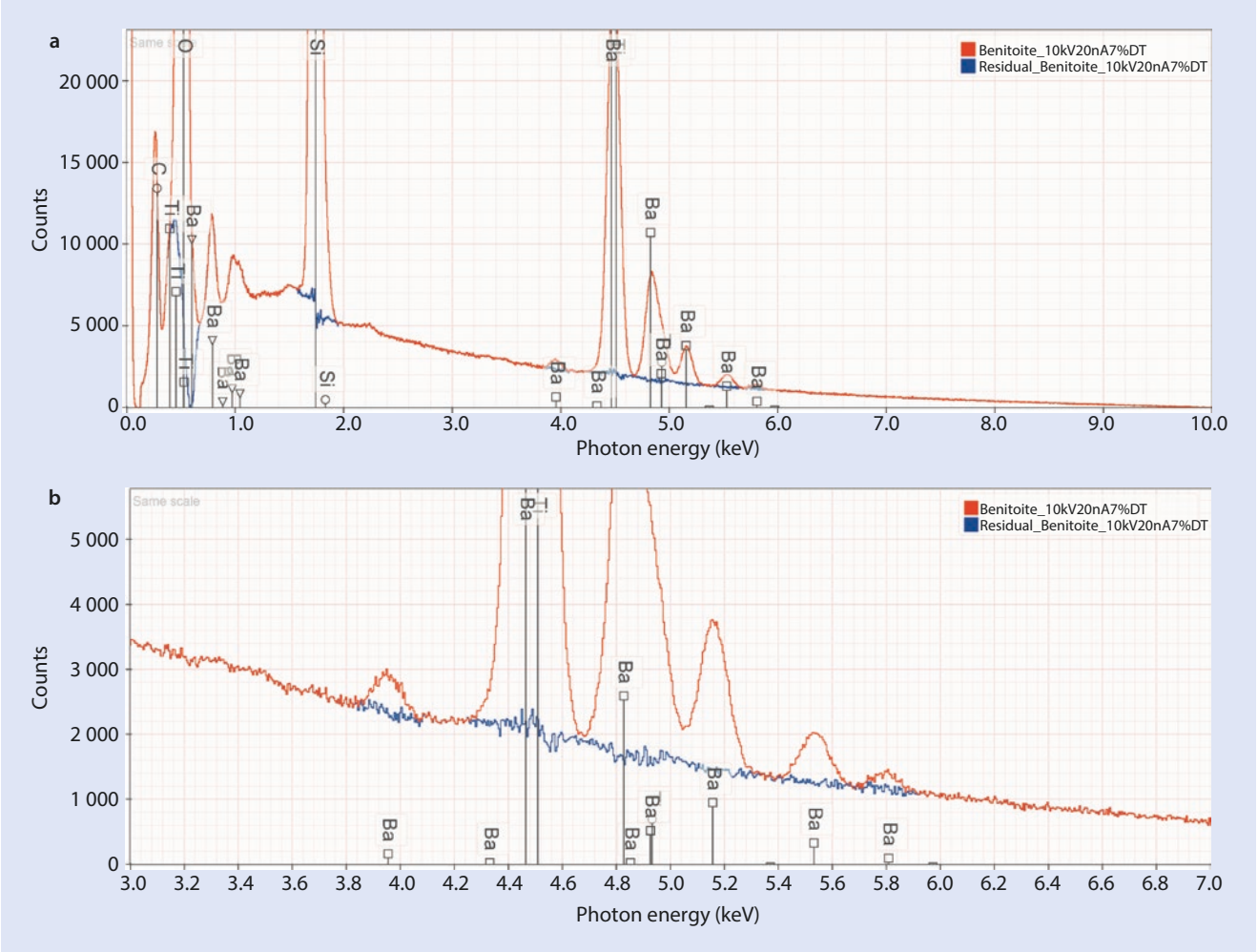

Fig. 20.7 **a** SDD-EDS spectrum of $BaTiSi_3O_9$ (benitoite) (*red*) at $E_0 = 10$ keV (11,137,000 counts) and residual (*blue*) after DTSA II analysis using $BaS_{i2}O_5$ (sanbornite) and Ti as fitting references and standards. **b** Expanded view

Table 20.7 Analysis of $BaTiSi_3O_9$ (benitoite) at $E_0 = 10$ keV with Ti and sanbornite ($BaSi_2O_5$) as fitting references and standards; integrated spectrum count = 11,366,000. Analysis performed with O K- $L_{2,3}$, Si K-$L_{2,3}$, Ti K-$L_{2,3}$ and Ba L_3-$M_{4,5}$

	O	Si	Ti	Ba
C_{av} (atom frac)	0.6416	0.2149	0.07096	0.07256
Z-correction	0.955	0.953	0.947	0.943
A-correction	0.804	1.041	0.989	1.004
F-correction	1	1	1.007	1
σ (7 replicates)	0.000269	0.00016	0.000176	0.000176
σ_{Rel} (%)	0.04 %	0.07 %	0.25 %	0.24 %
RDEV (%)	−0.20 %	0.28 %	−0.66 %	1.60 %
C (mass frac, single analysis)	0.3462	0.2032	0.1143	0.3356
Counting error, std	0.0002	0.0001	7.10×10^{-5}	0.0006
Counting error, unk	0.0002	0.0001	0.0004	0.0009
A-factor error	0.0142	0.0003	2.10×10^{-5}	3.50×10^{-5}
Z-factor error	0.0003	2.40×10^{-5}	1.10×10^{-6}	2.80×10^{-6}
Combined errors	0.0142	0.0003	0.0004	0.0011

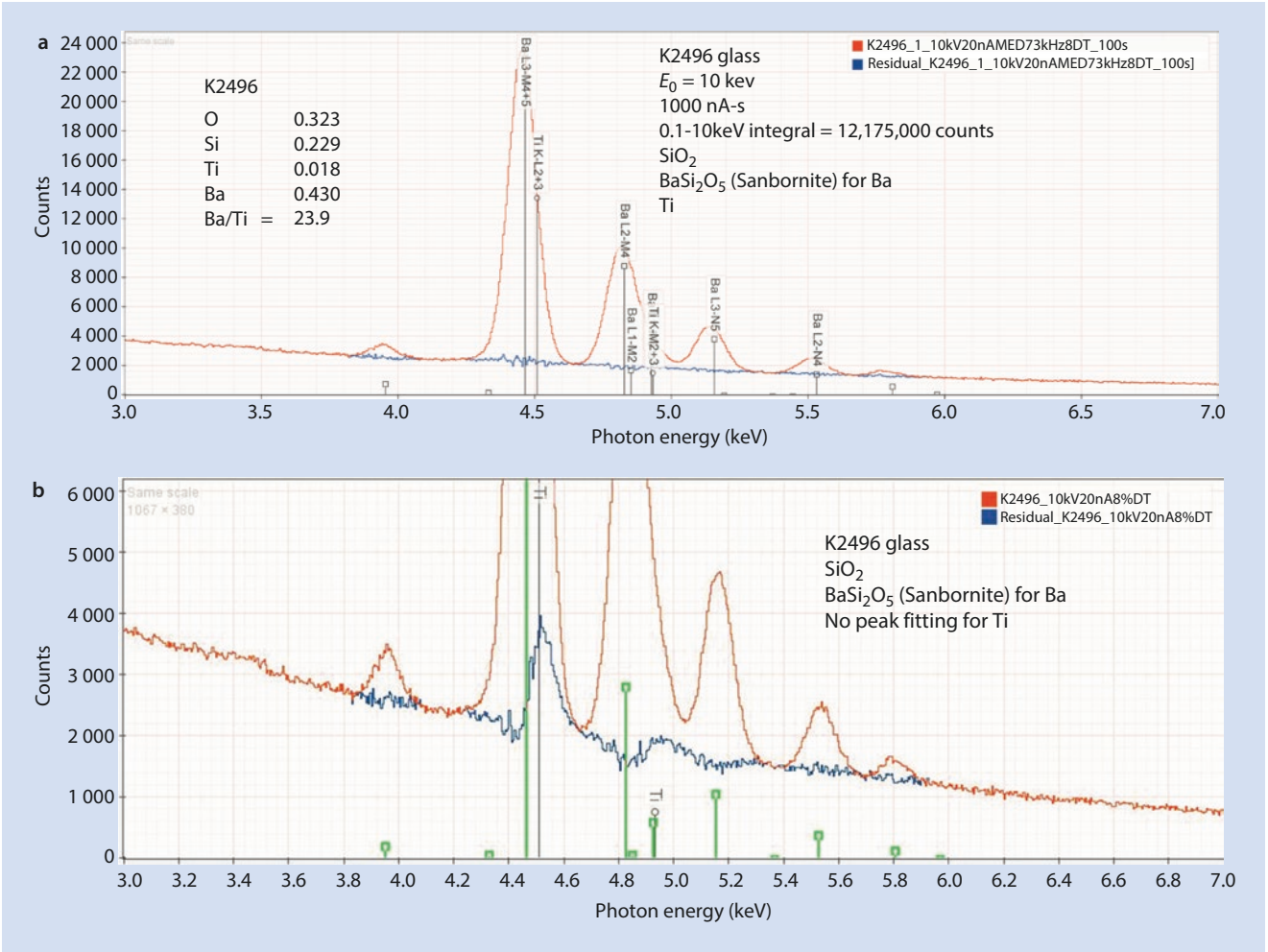

Fig. 20.8 **a** SDD-EDS spectrum of NIST microanalysis glass K2496 (*red*) at $E_0 = 10$ keV (12,175,000 counts) and residual (*blue*) after DTSA II analysis using $BaS_{i2}O_5$ (sanbornite) and Ti as fitting references and standards. **b** Same analysis protocol, but not including Ti in the peak-fitting. Note low level peaks for Ti K-$L_{2,3}$ and Ti K-M_3 (Ba L-family peaks marked as *green lines*)

Table 20.8 Analysis of NIST microanalysis glass K2496 at $E_0 = 10$ keV with Ti and sanbornite ($BaSi_2O_5$) as fitting references and standards; integrated spectrum count = 12,175,000. Analysis performed with O K- $L_{2,3}$, Si K-$L_{2,3}$, Ti K-$L_{2,3}$ and Ba L_3-$M_{4,5}$

	O	Si	Ti	Ba
C_{av} (atom frac)	0.6228	0.2585	0.01171	0.1069
Z-correction	0.984	0.983	0.983	0.98
A-correction	0.966	1.017	0.986	1.001
F-correction	1	1	1.01	1
σ (7 replicates)	0.000158	0.000277	0.000217	0.000226
σ_{Rel} (%)	0.03 %	0.11 %	1.80 %	0.21 %
RDEV (%)	−1.70 %	0.99 %	−0.64 %	8.70 %
C (mass frac)	0.3066	0.223	0.0177	0.4527
Counting error, std	0.0002	0.0002	1.10×10^{-5}	0.0008
Counting error, unk	0.0002	0.0001	0.0004	0.0007
A-factor error	0.0021	8.80×10^{-5}	3.90×10^{-6}	1.20×10^{-5}
Z-factor error	0.0003	2.70×10^{-5}	1.80×10^{-7}	4.00×10^{-6}
Combined errors	0.0021	0.0002	0.0004	0.0011

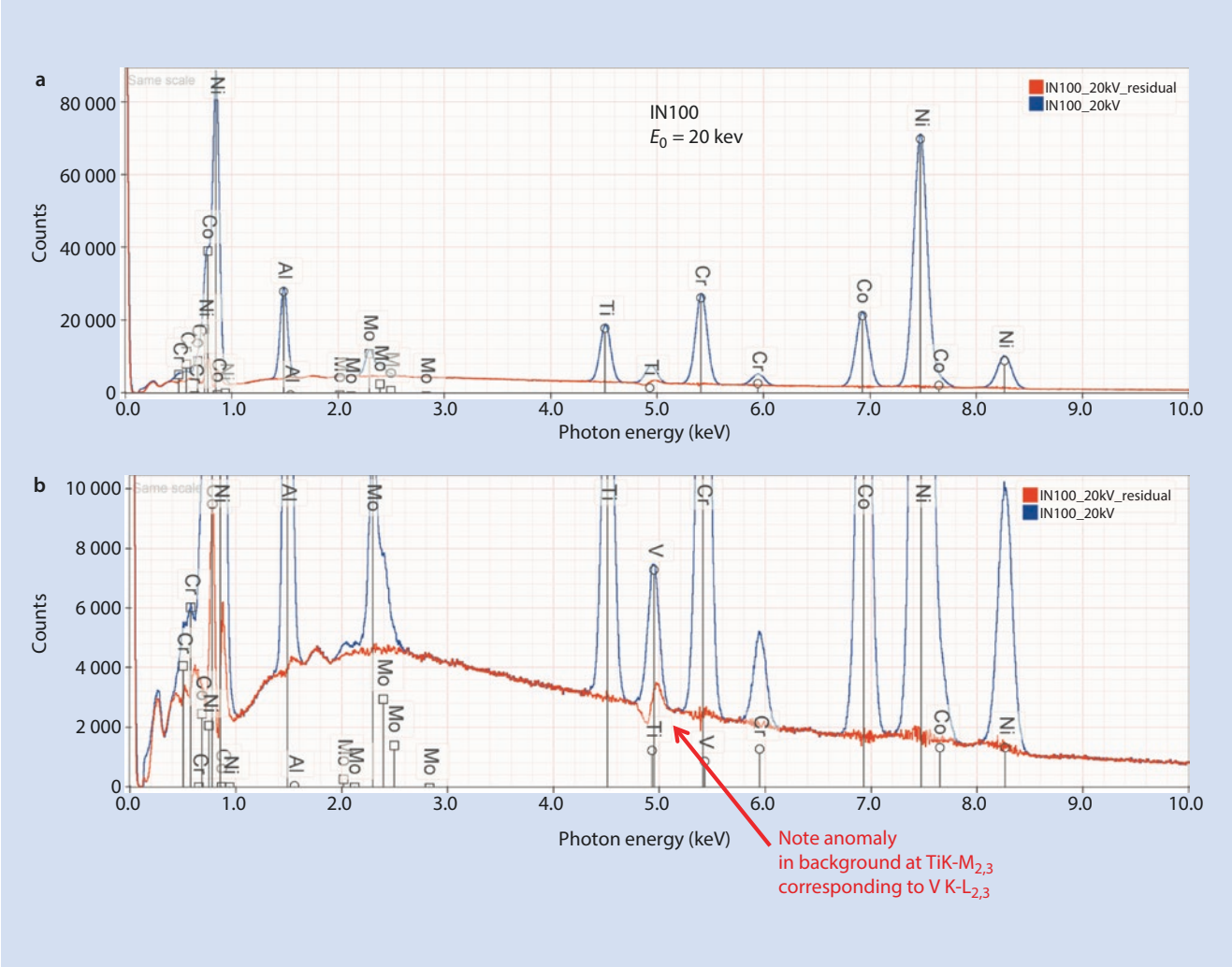

Fig. 20.9 Analysis of IN100 alloy fitting for Al, Ti, Cr, Co, Ni and Mo: **a** full spectrum (*blue*) and residual spectrum after peak-fitting (*red*); **b** expanded view, note anomaly in background at the energy of Ti K-M4,5 (4.931 keV), which closely corresponds to the energy of V K-L2,3 (4.952 keV)

Table 20.9 Analysis of IN100

	1st quantitative analysis	2nd quantitative analysis
Raw sum	0.9944 ± 0.0011	1.0032 ± 0.0013
Al	0.0559 ± 0.0007	0.0562 ± 0.0007
Ti	0.0473 ± 0.0001	0.0474 ± 0.0001
V		0.0110 ± 0.0002
Cr	0.0981 ± 0.0002	0.0949 ± 0.0006
Co	0.1551 ± 0.0003	0.1553 ± 0.0003
Ni	0.6065 ± 0.0008	0.6069 ± 0.0008
Mo	0.0315 ± 0.0002	0.0315 ± 0.0002

analysis (Table 20.9), despite the severe interference from the Ti constituent which has a concentration more than four times higher.

20.4.2 Analysis of a Stainless Steel

When is a Standard Not Suitable as a Peak-Fitting Reference?

One of the great strengths of the k-ratio/matrix correction protocol is simplicity of the required standards. Pure elements can be used for most of the periodic table, and for those elements that are not in a suitable solid form at ambient temperature and at the low chamber pressure, stoichiometric binary compounds that are stable under the beam can be used. This is an excellent situation for the analyst, since it is generally not possible to have a multi-element standard that is homogeneous on the microscopic scale and similar in

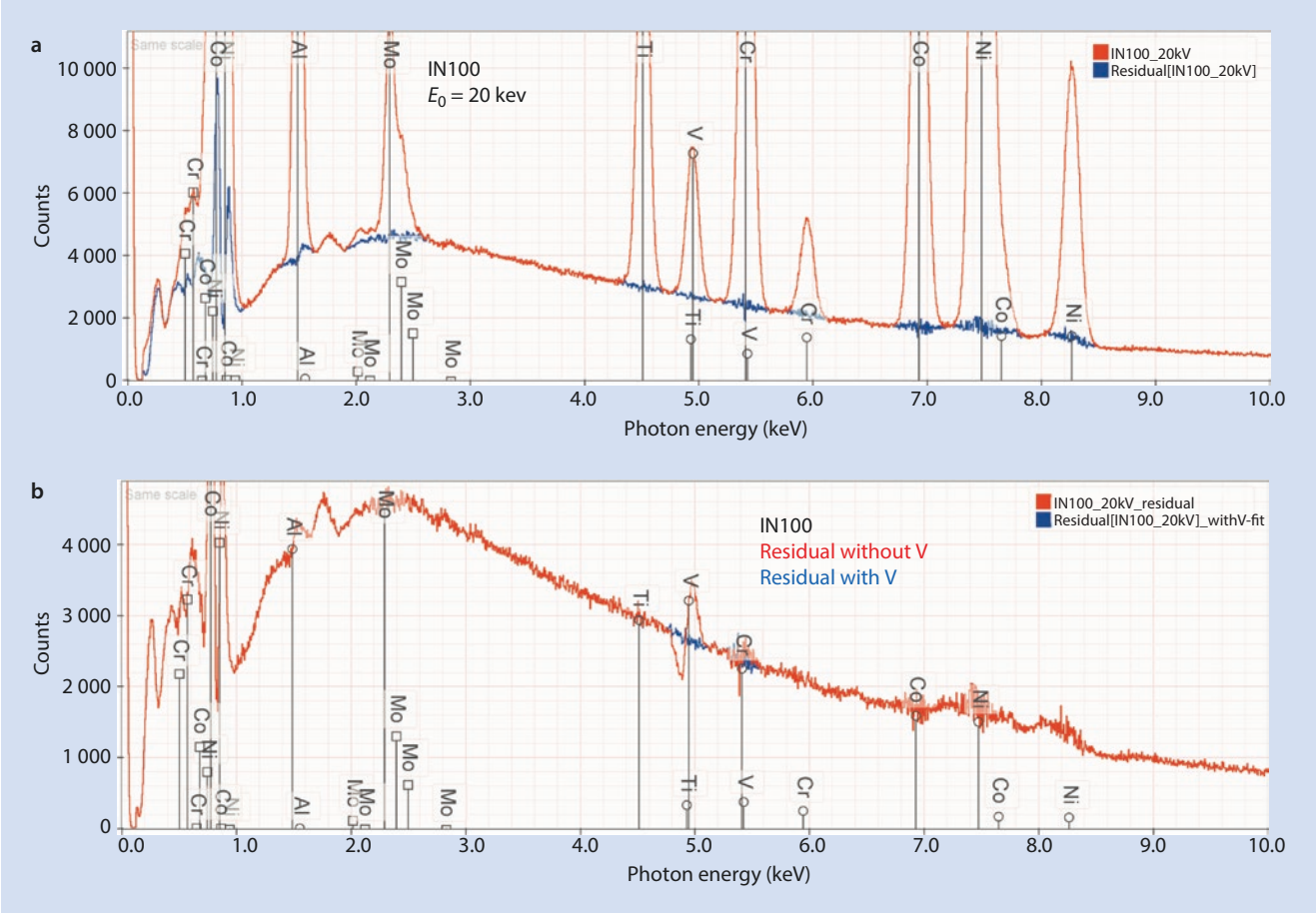

Fig. 20.10 **a** IN100 superalloy, fitting for Al, Ti, V, Cr, Co, Ni, and Mo. **b** Comparison of fitting residuals with and without inclusion of V; the background anomaly is eliminated

composition to a particular unknown specimen. For many simple binary as well as more complex mixtures of elements, Nature favors heterogeneity on the microscale, and many combinations of elements tend to phase separate to produce chemically heterogeneous microstructures. However, there are important cases where microscopically homogeneous, multi-element compositions are available, such as minerals, glasses, and a few metal alloys. An example is NIST Standard Reference Material 479, an Fe-Cr-Ni alloy which is certified to be homogeneous on a microscopic scale. SRM 479 can serve as a standard for the analysis of another more complex stainless steel. Figure 20.11 shows the spectrum of a type 316 stainless steel which the initial qualitative analysis shows that in addition to Cr, Fe, and Ni also contains peaks for Si and Mo. While SRM 479 is an ideal standard for this analysis of Cr, Fe, and Ni, it is not suitable to provide peak-fitting references for Cr, Fe, and Ni because of the mutual interference of these peaks. Thus, pure elements for Cr, Fe, and Ni are used for the peak-fitting references, while SRM 479 is used as the standard, reducing the magnitude of the matrix corrections because of the close similarity of the unknown and standard compositions. When the analysis is performed, including elemental Si and Mo as references and standards, the results given in Table 20.10 (column 2) are obtained. Close examination of the residual spectrum reveals the peaks of the Mn K-family. When the analysis is repeated including Mn in the suite of fitted elements, the results given in Table 20.10 (column 3) are obtained with a concentration of Mn = 0.0154, and the residual spectrum no longer contains anomalous peaks, as shown in Fig. 20.11c, d.

20.4.3 Progressive Discovery: Repeated Qualitative–Quantitative Analysis Sequences

Complex unknowns may require several iterations of qualitative and quantitative analysis to discover all of the constituents. For such situations, the analytical total as well as the residual spectrum serve as powerful guides to reach a successful result. As an example, consider the spectrum of a monazite (a lanthanum-cerium phosphate mineral) shown in Fig. 20.12a, b. The elements recognized in the first qualitative analysis stage are O, P, La, Ce (major) and Al, Si, Ca, and Th (minor). The first quantitative analysis round for these elements, with O calculated by stoichiometry, yielded

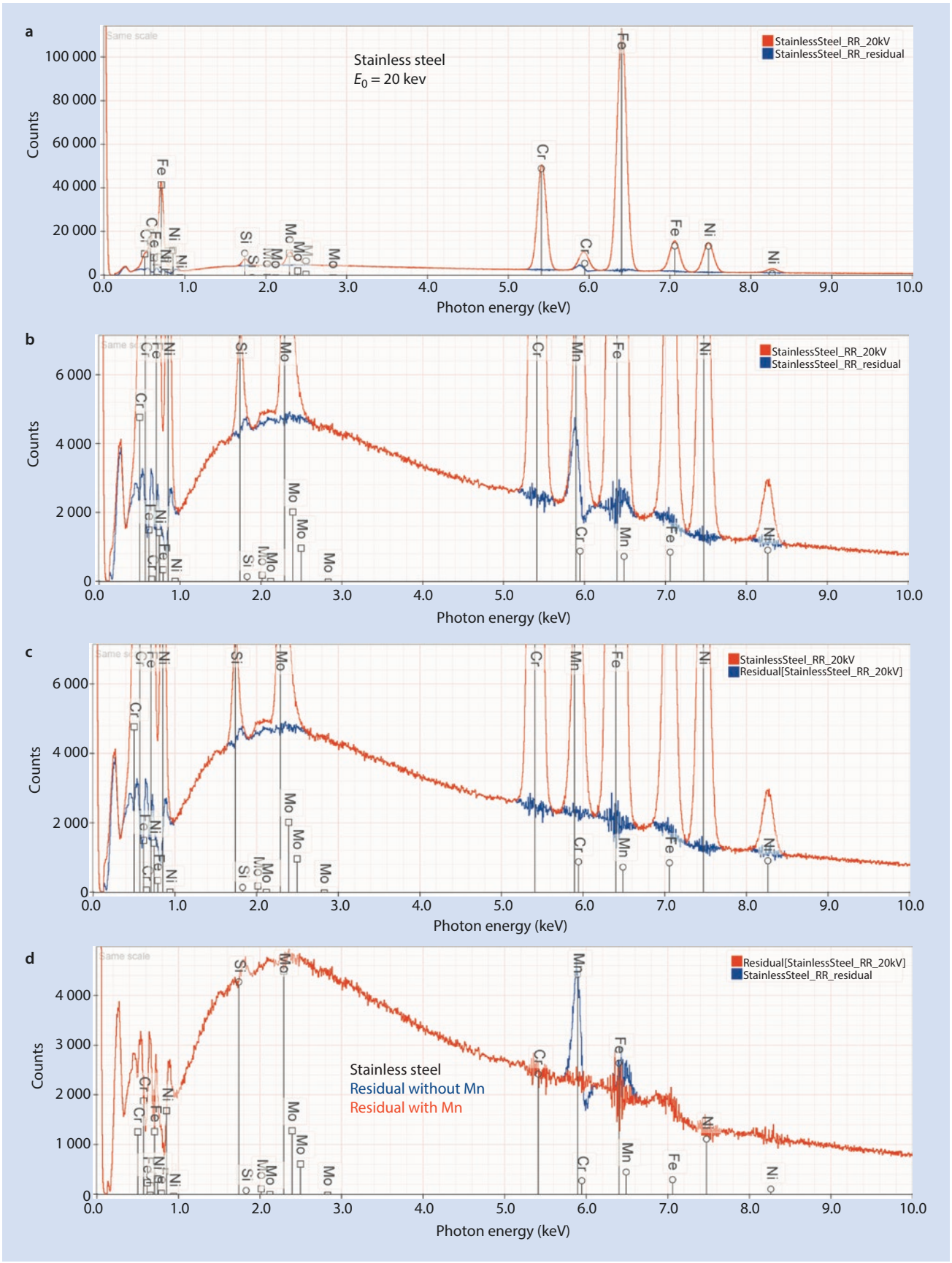

Fig. 20.11 **a** Stainless steel, fitting for Si, Cr, Fe, Ni, and Mo; residual in *blue*. **b** Expanded vertical scale, note detection of Mn. **c** Stainless steel, fitting for Si, Cr, Mn, Fe, Ni, and Mo; residual in *blue*. **d** Comparison of residuals with fitting for Mn (*red*) and without (*blue*)

Table 20.10 Analysis of a type 316 stainless steel (mass concentrations)

	1st quantitative analysis	2nd quantitative analysis
Raw sum	0.9861 ± 0.0009	1.0031 ± 0.0009
Si	0.0053 ± 0.0001	0.0053 ± 0.0001
Cr	0.1705 ± 0.0003	0.1711 ± 0.0003
Mn		0.0154 ± 0.0002
Fe	0.6539 ± 0.0006	0.6545 ± 0.0006
Ni	0.1328 ± 0.0005	0.1330 ± 0.0005
Mo	0.0237 ± 0.0002	0.0238 ± 0.0002

the results listed in Table 20.11 (first analysis). The analytical total is anomalously low at 0.7635. The second round of qualitative analysis of the fitting residuals from the first quantitative analysis in Fig. 20.12c–e shows several new peaks that are identified: Sr, Y, and Zr in the P region and Ti, Pr, and Nd in the La-Ce region. When these elements are included in the second round of quantitative analysis, as listed in Table 20.11, the analytical total increases to 0.9629. The third round of qualitative analysis of the fitting residuals from the second quantitative analysis in Fig. 20.12f,g shows Nb in the P region and Sm and Fe in the La-Ce region. After the third round of quantitative analysis, the analytical total increases to 0.9960, and the third round residuals are shown in Fig. 20.12h, i superimposed on the residuals from rounds one and two, indicating only minor changes between rounds two and three. Should this analysis be repeated for a fourth round? The level of Nb that has been measured is only 0.0006 (600 ppm), and the confidence is this level is low. There remain some low level structures in the third analysis residuals, but to take this analysis further, the spectrum should be measured for additional time to increase the total count at least by a factor of four.

20.5 Is the Specimen Homogeneous?

For the most part, Nature seems to prefer heterogeneity on a microscopic scale. That is, many combinations of two or more elements spontaneously form two or more phases, where a phase is defined as matter that is distinct in chemical composition and physical state, thus creating a chemical microstructure. Indeed, the great value of electron excited X-ray microanalysis is its capability to measure elemental composition on the spatial scale of a micrometer and finer to characterize this chemical microstructure.

As part of an effective analysis strategy, it is generally wise to make multiple measurements of each distinct region of interest of a specimen rather than just a single measurement. When a material is sampled at multiple locations under carefully controlled, reproducible analytical conditions, there will inevitably be variations in the results due to the natural statistical fluctuations in the numbers of measured X-rays, both for the characteristic and continuum background of the specimen and the standard. The question often arises when examining the variations in such replicate results if the material can be regarded as homogeneous or if the degree of variation in the results is indicative of actual specimen heterogeneity.

In electron-excited X-ray microanalysis, what is of ultimate importance is the precision of the composition rather than just that of an individual intensity measurement for an element. This point has been discussed in detail by Ziebold (1967) and Lifshin et al. (1999). Note first that a k ratio consists actually of the averages of four measurements: N_{sam}, the mean intensity measured on the sample; $N_{sam}(B)$, the corresponding mean background at the same energy; N_{stan}, the intensity measured on the standard; and $N_{stan}(B)$, the corresponding background for the standard:

$$k = \left[N_{sam} - N_{sam}(B) \right] / \left[N_{stan} - N_{stan}(B) \right] \quad (20.4)$$

In reality a single measurement of each of the four terms in Eq. (20.4) results in only a single estimate of k and many sets of measurements are required to approach the true mean value of k.

For multiple determinations of the k-ratio, Ziebold (1967) showed that the precision in the k-ratio (σ_k) is given by

$$\sigma_k^2 = k^2 \left\{ \begin{array}{l} \left[\left(N_{sam} + N_{sam}(B) \right) / \left[n_{sam} \left(N_{sam} - N_{sam}(B) \right)^2 \right] \right] \\ + \left[\left(N_{stan} + N_{stan}(B) \right) / n_{stan} \left(N_{stan} - N_{stan}(B) \right)^2 \right] \end{array} \right\} \quad (20.5)$$

where N represents the mean of the set of measurements for each parameter, for example:

$$N_{sam} = \sum_i^n N_i / n_{sam} \quad (20.6)$$

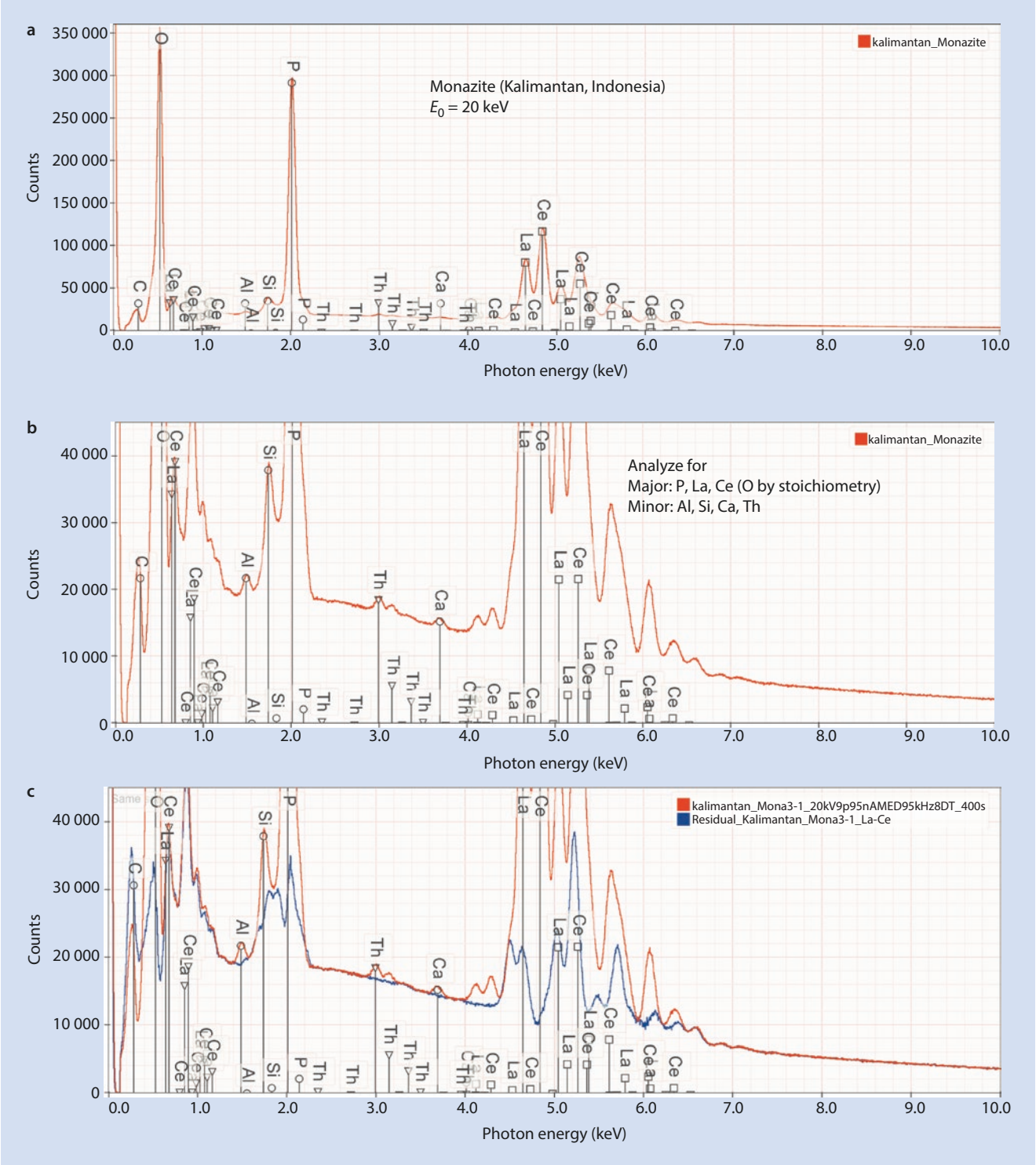

Fig. 20.12 Monazite (lanthanum-cerium phosphate mineral) at E_0 = 20 keV; 0.1 keV to 30 keV = 48.7 million counts: **a** original spectrum; **b** vertical expansion; **c** Round 1: full spectrum residuals after first quantitative analysis; **d** P-region, first residuals; **e** La-Ce-region, first residuals; Round 2: **f** P-region, second residuals; **g** La-Ce-region, second residuals; Round 3; **h** P-region, all residuals; **i** La-Ce-region, all residuals

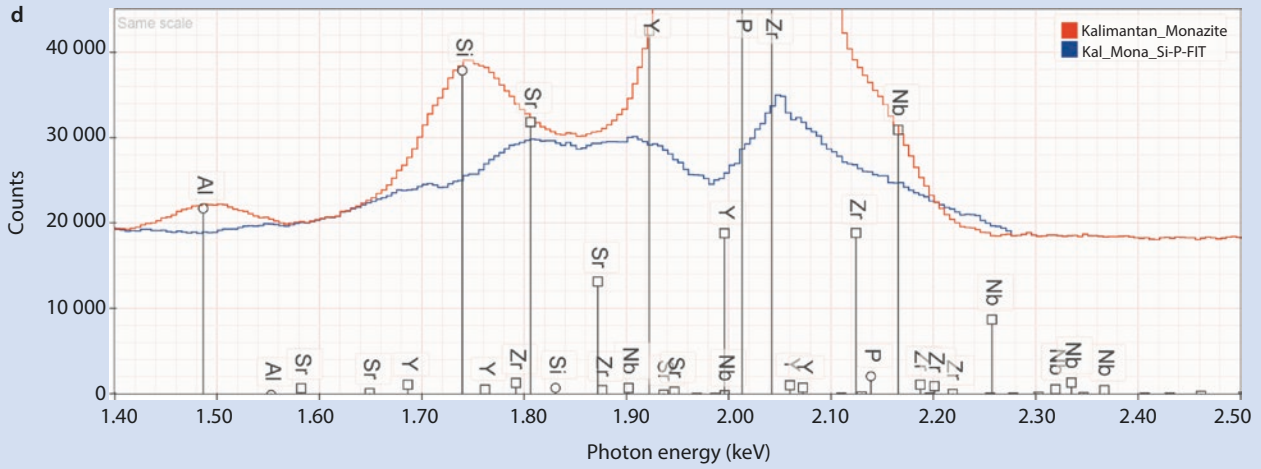

Fig. 20.12 (continued)

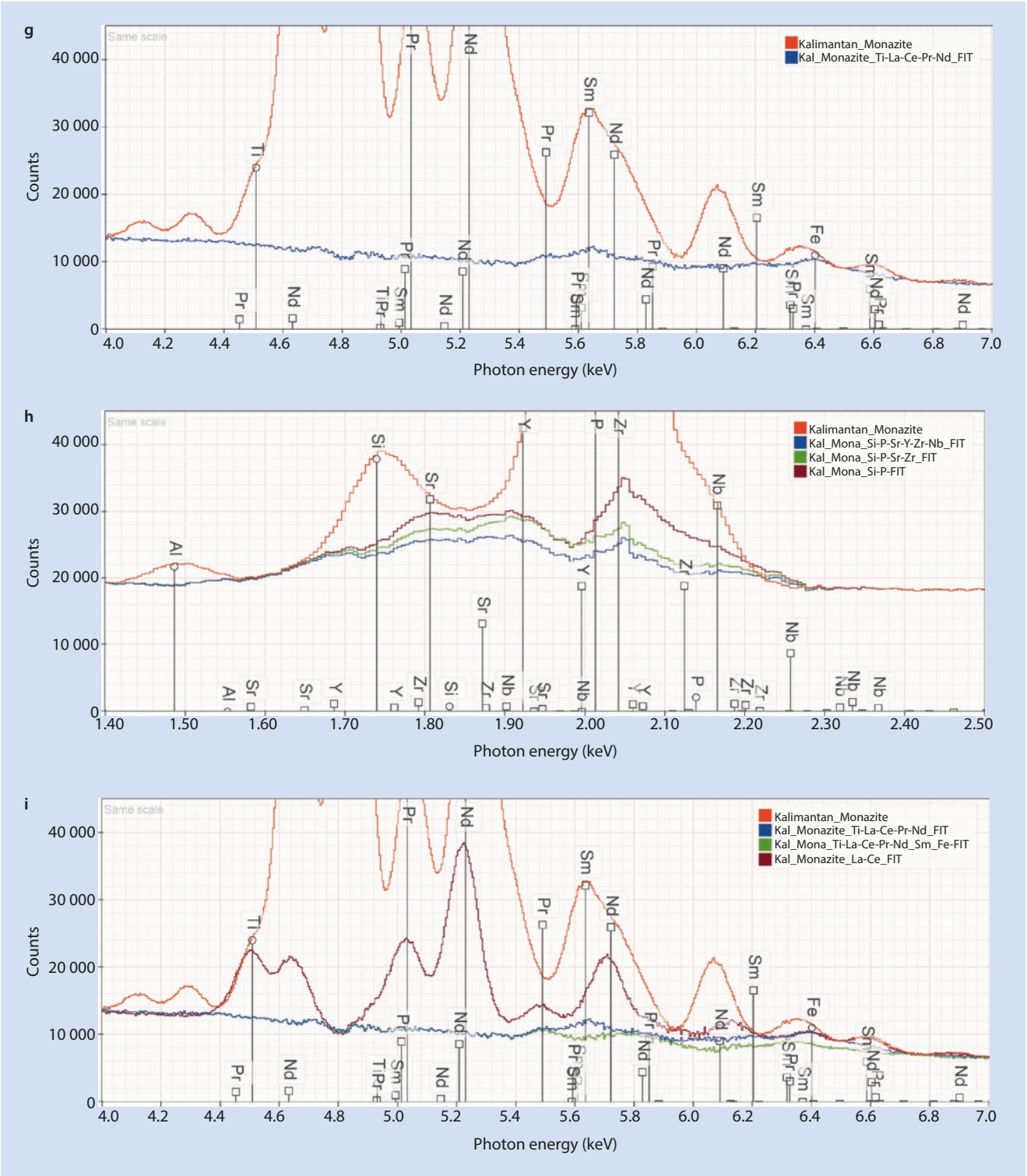

Fig. 20.12 (continued)

Table 20.11 Analysis of a monazite

Round	O (by assumed stoichiometry)	Al	Si	P	Ca	Ti
First analysis	0.2363 ± 0.0008	0.0013 ± 0.0000	0.0049 ± 0.0000	0.1114 ± 0.0006	0.0007 ± 0.0000	
Second analysis	0.2828 ± 0.0009	0.0016 ± 0.0000	0.0059 ± 0.0001	0.1240 ± 0.0007	0.0007 ± 0.0000	0.0071 ± 0.0001
Third analysis	0.2908 ± 0.0010	0.0015 ± 0.0000	0.0061 ± 0.0001	0.1263 ± 0.0007	0.0007 ± 0.0000	0.0072 ± 0.0001
Element	Fe	Sr	Y	Zr	Nb	La
First analysis						0.1359 ± 0.0002
Second analysis		0.0016 ± 0.0001	0.0098 ± 0.0002	0.0113 ± 0.0002		0.1585 ± 0.0003
Third analysis	0.0022 ± 0.0001	0.0028 ± 0.0001	0.0030 ± 0.0002	0.0117 ± 0.0002	0.0006 ± 0.0001	0.1591 ± 0.0003
Element	Ce	Pr	Nd	Sm	Th	Raw Sum
First analysis	0.2692 ± 0.0004				0.0038 ± 0.0001	0.7635 ± 0.0011
Second analysis	0.2699 ± 0.0004	0.0221 ± 0.0003	0.0750 ± 0.0003		0.0040 ± 0.0001	0.9629 ± 0.0013
Third analysis	0.2709 ± 0.0004	0.0221 ± 0.0003	0.0751 ± 0.0003	0.0073 ± 0.0005	0.0040 ± 0.0001	0.9960 ± 0.0030

and n_{sam} and n_{stan} are the numbers of measurements of the sample and standard. The corresponding precision in the measurement of the concentration is given by

$$\sigma_C^2 = C^2 \left\{ \left[\left(N_{sam} + N_{sam}(B) \right) / n_{sam} \left(N_{sam} - N_{sam}(B) \right)^2 \right] + \left[\left(N_{stan} + N_{stan}(B) \right) / n_{stan} \left(N_{stan} - N_{stan}(B) \right)^2 \right] \right\} \left\{ 1 - \left[(a-1) C / a \right] \right\}^2 \quad (20.7)$$

where the parameter "a" is the constant in the hyperbolic relation (Ziebold and Ogilvie 1964):

$$(1-k)/k = a\left[(1-C)/C\right] \quad (20.8)$$

The parameter "a" can be calculated using Eq. (20.8) with the measured value of k and the calculated value of C from the quantitative analysis software results.

Equation 20.4 makes it possible to assess statistical uncertainty in an estimate of composition. For example, it can be used to construct a confidence interval (e.g., ± 1.96σ_C gives the 95 % confidence interval) for the difference of two samples or to plan how many counts must be collected to be able to estimate differences between two samples at the desired level of precision. The calculation of the confidence interval is based on the normal distribution of the estimate of C for large samples. This confidence interval is only based on the statistical uncertainty inherent in the X-ray counts. The full error budget requires also estimating the uncertainty in the principal matrix corrections for absorption (A) and scattering/energy loss (Z) (Ritchie and Newbury 2012). NIST DTSA-II provides these error estimates in addition to the error in the measurement of the k-ratio.

The use of Eq. (20.7) to calculate σ_c for an alloy with a composition of 0.215-Mo_0.785-W (21.5 wt % Mo and 78.5 wt % W) and the spectrum shown in Fig. 20.13 is as follows:

First determine the number of Mo L_3-M_5 and W L_3-M_5 counts measured on the sample and standard as well as the corresponding background counts for each:

At $E_0 = 20$ keV and $i_B = 10$ nA for an SDD-EDS of $\Omega = 0.0077$ sr, the spectrum of the alloy and the residual after peak-fitting, as shown in Fig. 20.13, gives the following intensities for a single measurement:

Mo L_3-M_5	bkg	W L_3-M_5	bkg
884416	195092	868516	111279

The pure element standards gave the following values for a single measurement:

7016889	211262	1147787	134382

These intensities yield the following mean k-values:

0.1260	0.7567

From the NIST DTSA-II results and Eq. (20.6):

Mo $k = 0.1235$ $C = 0.2132$ (normalized $C = 0.2148$) $a = 1.92$
W $k = 0.7540$ $C = 0.7792$ (normalized $C = 0.7852$) $a = 1.15$

Substituting these values in Eq. (20.4) gives

Mo	W
$\sigma_C = 0.0003$	$\sigma_C = 0.0012$

Thus, from the statistics of the X-ray counts measured for the alloy and the pure element standards, the 95 % confidence limit for *reproducibility* is given by ± 1.96σ_C

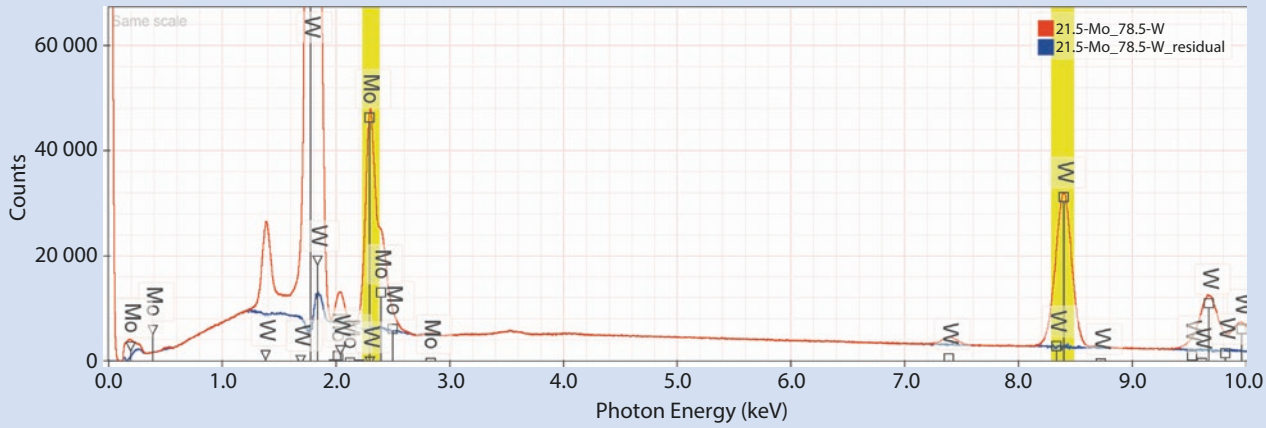

Fig. 20.13 EDS spectrum of 0.215-Mo, 0.785-W alloy showing the residuals after peak fitting; $E_0 = 20$ keV

Table 20.12 Analysis of 0.215-Mo_0.785-W alloy (normalized mass fractions) (analysis in bold used for the calculations above)

Mo	W
0.2166	0.7834
0.2148	0.7852
0.2141	0.7859
0.2177	0.7823
0.2185	0.7815
0.2180	0.7820
0.2175	0.7825
0.2203	0.7797
0.2275	0.7725
0.2312	0.7688
0.2346	0.7654
0.2363	0.7637
0.2358	0.7642
0.2344	0.7656
0.2389	0.7611

Mo $C = 0.2148 \pm 0.0006$ or $0.215 \pm 0.28\,\%$
W $C = 0.7852 \pm 0.0024$ or $0.785 \pm 0.31\,\%$

If multiple locations are measured under consistent measurement conditions—e.g., constant beam energy, beam current, and EDS performance—then values that fall outside the ranges given for Mo and W are indicative of heterogeneity, that is, real deviations in the composition of the alloy. Table 20.12 lists 15 measurements on this alloy made at randomly selected locations, which reveal significant heterogeneity with the most extreme excursion approximately 11 % in the Mo constituent from the ideal values. This deviation is well outside that expected from natural variations due to statistical fluctuations in the measured counts as calculated above.

The full uncertainty budget reported by DTSA-II, including the estimates for the uncertainties in the A and Z matrix corrections as well as the X-ray statistics is

Mo	W
$\sigma_C = 0.0039$	$\sigma_C = 0.0017$

The large increase in σ_C for Mo beyond the contribution of the X-ray statistics is due to the contribution of the matrix correction factor for absorption, $A = 0.528$.

20.6 Beam-Sensitive Specimens

In some cases, the interaction of the electron beam can damage the specimen and locally alter the composition, often with the effects showing a strong dependence on the total dose, the dose per unit volume, and the dose rate.

20.6.1 Alkali Element Migration

In some insulating materials, especially non-crystalline materials such as glasses, alkali family elements can migrate in response to the local charge injected below the surface by the beam, even when a thin conducting surface layer such as carbon has been applied to discharge the specimen. Migration typically leads to diminishing alkali concentration with time in the excited volume. The phenomenon can be detected by measuring a time series of spectra and carefully comparing the intensity of alkali element peaks to stable matrix peaks such as that of Si, as shown in Fig. 20.14 for "Corning glass A" which has a high alkali composition with approximately 10 weight percent Na and 2.4 weight percent potassium (listed in Table 20.11) (Vicenzi et al. 2002). Each spectrum shown in Fig. 20.14 was recorded for 10 s with a fixed, focused beam, which creates the maximum possible dose per unit volume.

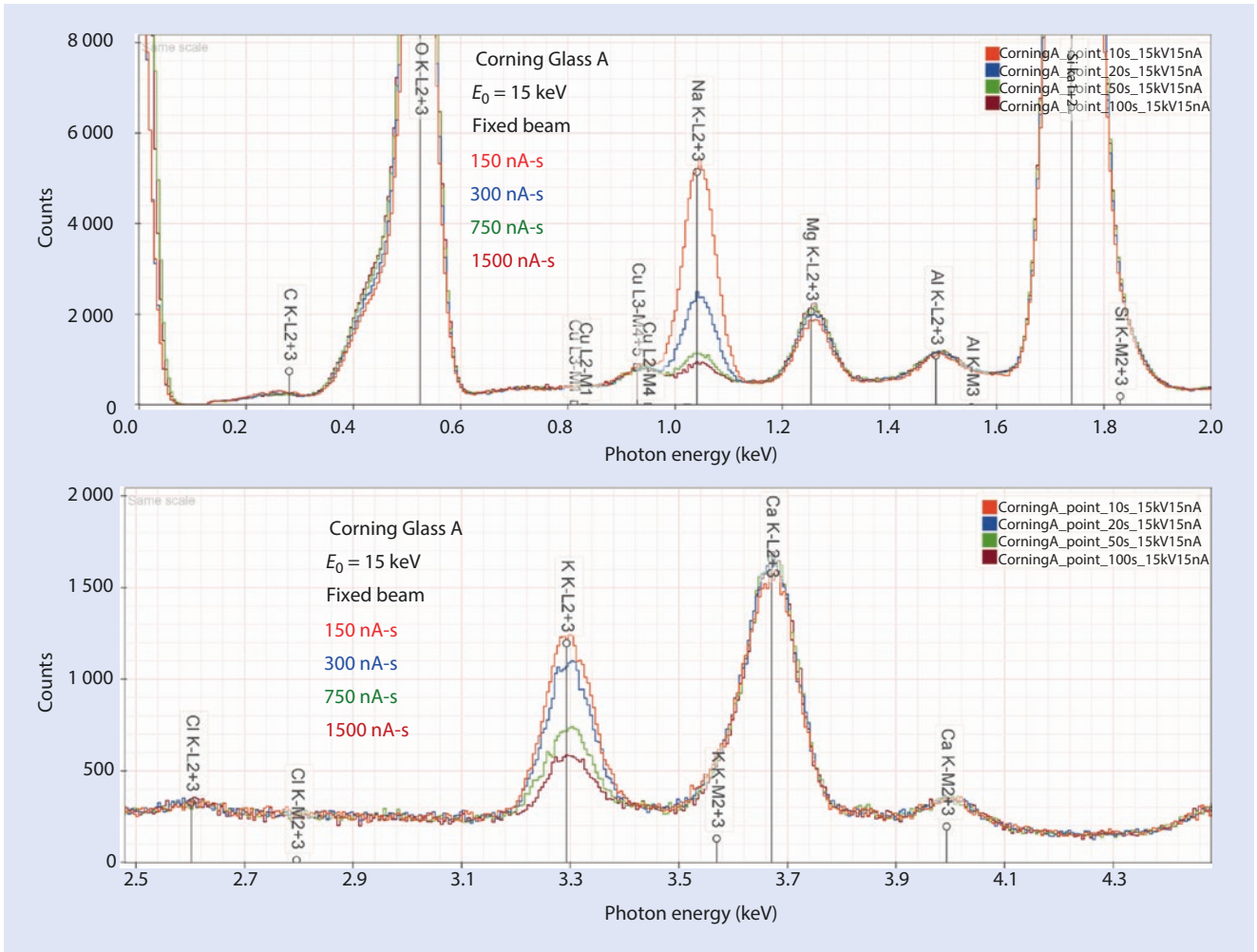

Fig. 20.14 Corning glass A, showing Na and K migration as a function of dose for a fixed beam (15 keV, 15 nA)

Comparing the first (150-nA-s dose) and the second spectra (300-nA-s dose), the Na intensity is seen to fall by more than a factor of two as the dose increases, while the K intensity diminishes by approximately 20 %. After a dose of 1500 nA-s, the Na peak is reduced to approximately 10 % of its intensity after 10 s, while the K peak decreases to approximately 25 % of its original value, whereas other non-alkali elements—e.g., Mg, Al, Ca, Si, etc.—remain nearly constant with dose. Even this time series is somewhat misleading. If the initial dose is reduced by a factor of 10, the Na intensity observed is higher by approximately 30 %, as shown in Fig. 20.15, while the K intensity is higher by approximately 5 %. At the extremely high volumetric dose created by the fixed point beam in these experiments, significant alkali migration occurs even with the initial short beam dwell (e.g., 1 s, 15 nA). The effects of the dose on the results obtained by quantitative analysis with DTSA-II are given in Table 20.13. Even in the first analysis (150 nA-s dose), the measured Na concentration is a factor of 2 lower than the synthesized glass composition, and after the maximum dose utilized for this series (1500 nA-s dose), the Na concentration has decreased by a factor of 11.

Methods to reduce alkali element migration are based on modifying the total dose, the dose per unit area (and volume), and/or the dose rate. Reducing the dose per unit area is often one of the most effective ways to control migration. By defocusing the fixed beam or by scanning the focused beam rapidly over a large area, the dose per unit area can be greatly reduced, often by several orders of magnitude, compared to a fixed, focused beam. Because of the basic assumption of the k-ratio/matrix correction protocol that the material being analyzed must have the same composition over the entire volume excited by the electron beam, this increased-area strategy is only valid providing the region of analytical interest is homogeneous over a sufficiently large to accommodate the defocused or rapidly scanned beam. The effect of increasing the scanned area is shown in Fig. 20.16 for Corning glass A, where the measured Na intensity increases rapidly as the scanned area is increased. Table 20.14 compares DTSA-II quantitative analyses of spectra with the same dose (15 keV, 1500 nA-s) obtained with a point beam and with that beam rapidly scanning over an area 100 μm square. The scanned area results correspond very closely to the as-synthesized

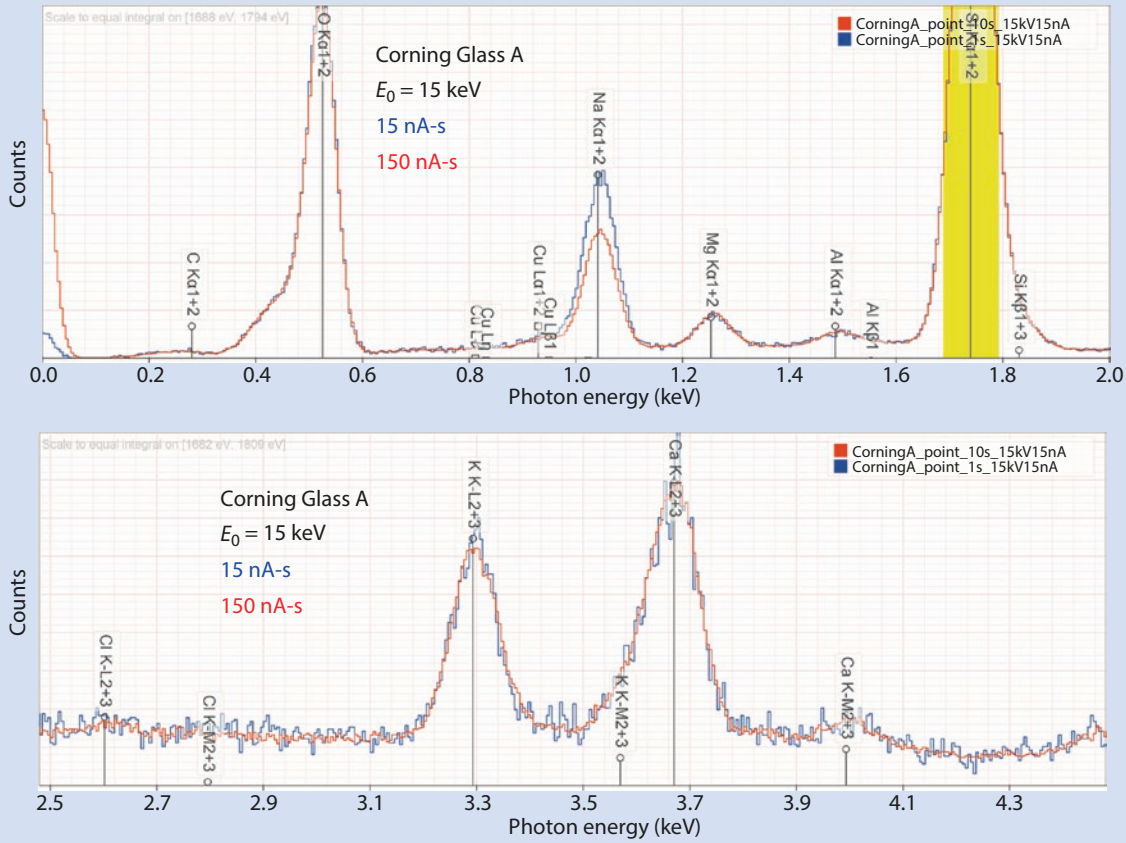

Fig. 20.15 Corning glass A, showing Na and K migration compared as a function of dose with a reduction of a factor of 10 difference for a fixed beam (15 keV, 15 nA); spectra normalized to the Si peak

Table 20.13 DTSA-II analysis of Corning Glass A (E_0 = 15 keV), oxygen by assumed stoichiometry, fixed beam

Element	As-synthesized mass conc	150 nA-s raw mass conc	300 nA-s raw mass conc	750 nA-s raw mass conc	1500 nA-s raw mass conc
O	0.4421	0.4316 ± 0.0009	0.4313 ± 0.0009	0.4496 ± 0.0009	0.4644 ± 0.0009
Na	0.1061	0.0519 ± 0.0004	0.0364 ± 0.0004	0.0172 ± 0.0003	0.0098 ± 0.0003
Mg	0.0160	0.0161 ± 0.0002	0.0161 ± 0.0002	0.0178 ± 0.0002	0.0186 ± 0.0002
Al	0.0529	0.0050 ± 0.0001	0.0051 ± 0.0001	0.0052 ± 0.0001	0.0058 ± 0.0001
Si	0.3111	0.3192 ± 0.0006	0.3230 ± 0.0007	0.3438 ± 0.0007	0.3574 ± 0.0007
K	0.0238	0.0251 ± 0.0003	0.0230 ± 0.0003	0.0195 ± 0.0003	0.0166 ± 0.0003
Ca	0.0359	0.0363 ± 0.0003	0.0364 ± 0.0003	0.0381 ± 0.0003	0.0386 ± 0.0003
Ti	0.00474	0.0053 ± 0.0002	0.0059 ± 0.0002	0.0057 ± 0.0002	0.0057 ± 0.0002
Mn	0.00775	0.0086 ± 0.0003	0.0084 ± 0.0003	0.0091 ± 0.0003	0.0101 ± 0.0003
Fe	0.00762	0.0083 ± 0.0003	0.0082 ± 0.0003	0.0074 ± 0.0003	0.0090 ± 0.0003
Cu	0.00935	0.0098 ± 0.0005	0.0104 ± 0.0005	0.0112 ± 0.0005	0.0108 ± 0.0005
Sn	0.00150	0.0030 ± 0.0008	0.0034 ± 0.0007	0.0036 ± 0.0007	0.0054 ± 0.0007
Sb	0.0146	0.0124 ± 0.0007	0.0140 ± 0.0007	0.0139 ± 0.0007	0.0140 ± 0.0007
Ba	0.0050	0.0045 ± 0.0005	0.0036 ± 0.0005	0.0056 ± 0.0005	0.0042 ± 0.0005
Raw total		0.938	0.926	0.9485	0.9718

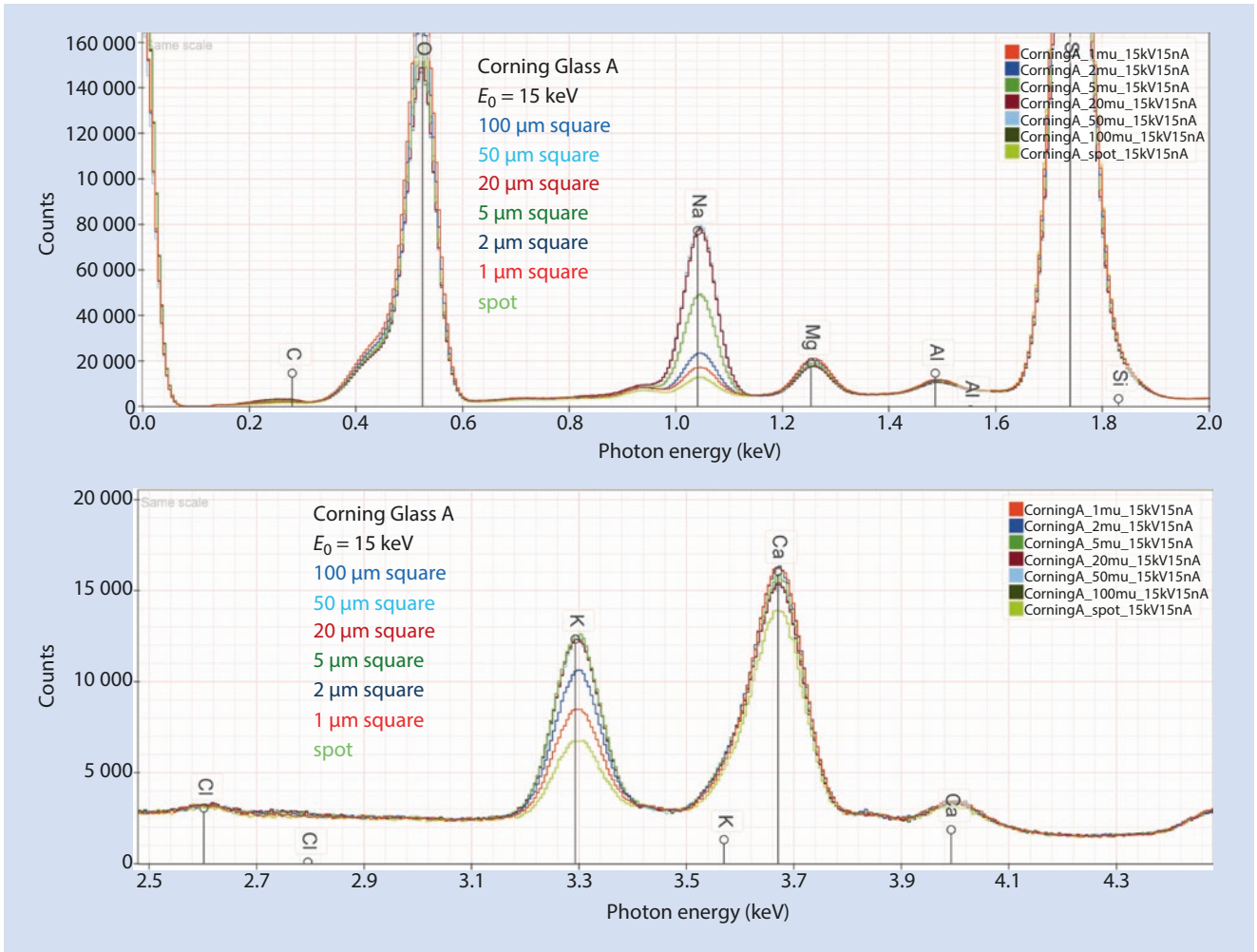

Fig. 20.16 Corning glass A, showing Na and K migration as a function of dose for scanning beams covering various areas (20 keV, 10 nA)

values for the glass, including the alkali elements Na and K, whereas the point beam results show reductions in the Na and K concentrations. Figure 20.17 shows that the measured sodium and potassium concentrations increase to reach the synthesized values as the scanned area dimensions are increased to cover areas above 20 x 20-µm (nominal magnification 5 kX) for the particular dose utilized (15 keV, 1500 nA-s). Thus, while scanning a large homogeneous area obviously concedes the spatial resolution capability of electron-excited X-ray microanalysis, this approach may be the most expedient technique to control and minimize alkali element migration.

Materials that can serve as useful standards for sodium include certain crystalline minerals such as albite ($NaAlSi_3O_8$) in which the sodium is much more stable under electron bombardment. However, even for albite the use of a stationary high intensity point beam may produce significant migration effects, as shown in Fig. 20.18 for spectra collected with a stationary point beam as a function of dose (upper) and at the same dose with a fixed beam and two different sizes of scanned areas (lower). Thus, the use of a scanned area rather than a fixed beam may be necessary when collecting a standard spectrum, even on a crystalline material.

20.6.2 Materials Subject to Mass Loss During Electron Bombardment—the Marshall-Hall Method

Thin Section Analysis

The X-ray microanalysis of biological and polymeric specimens is made difficult, and sometimes impossible, by several forms of radiation damage that are directly caused by the electron beam. At the beam energies used in the SEM (0.1–30 keV), it is possible for the kinetic energy of individual beam electrons to break and/or rearrange chemical bonds. The radiation damage can release smaller molecules such as

Table 20.14 DTSA-II quantitative analysis of Corning glass A: Comparison of results with a fixed beam and scanned beam (100 μm square) (15 keV/15 nA); oxygen by assumed stoichiometry

Element	As-synthesized mass conc	1500 nA-s (fixed beam) raw mass conc	1500 nA-s (100-μm^2 scan) raw mass conc
O	0.4421	0.4644 ± 0.0009	0.4577 ± 0.0006
Na	0.1061	0.0098 ± 0.0003	0.1076 ± 0.0004
Mg	0.0160	0.0186 ± 0.0002	0.0164 ± 0.0001
Al	0.0529	0.0058 ± 0.0001	0.0056 ± 0.0000
Si	0.3111	0.3574 ± 0.0007	0.3239 ± 0.0005
K	0.0238	0.0166 ± 0.0003	0.0257 ± 0.0002
Ca	0.0359	0.0386 ± 0.0003	0.0350 ± 0.0001
Ti	0.00474	0.0057 ± 0.0002	0.0051 ± 0.0001
Mn	0.00775	0.0101 ± 0.0003	0.0082 ± 0.0001
Fe	0.00762	0.0090 ± 0.0003	0.0077 ± 0.0001
Cu	0.00935	0.0108 ± 0.0005	0.0096 ± 0.0003
Sn	0.00150	0.0054 ± 0.0007	0.0045 ± 0.0003
Sb	0.0146	0.0140 ± 0.0007	0.0125 ± 0.0002
Ba	0.0050	0.0042 ± 0.0005	0.0042 ± 0.0002
Raw total		0.9718	1.0254

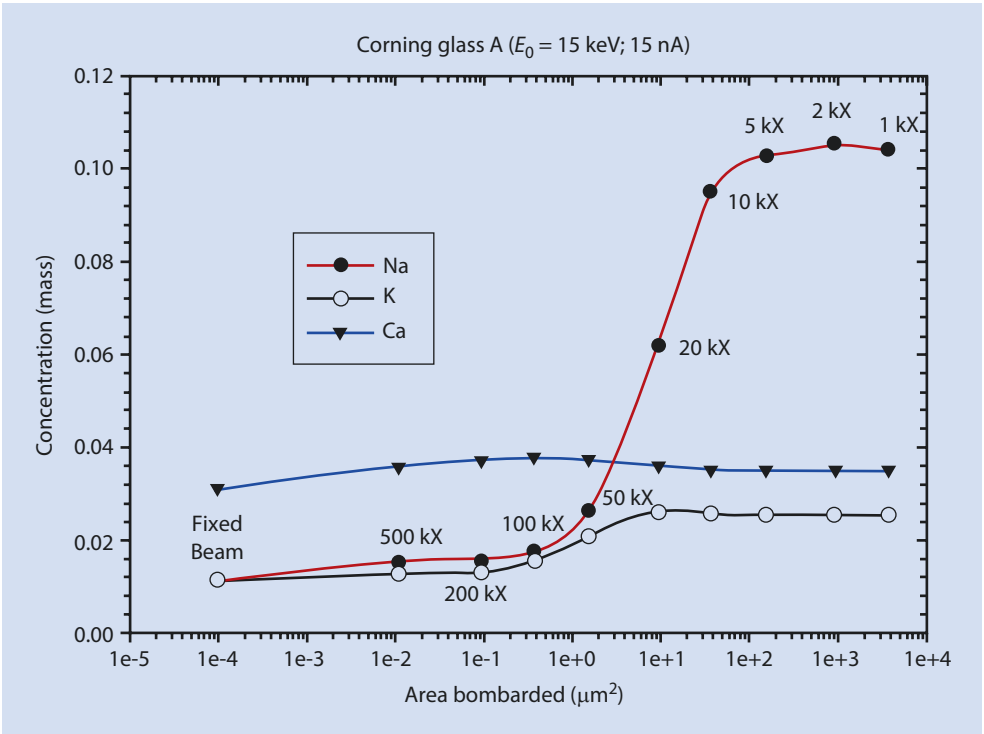

Fig. 20.17 Results of quantitative analysis of Corning glass A as a function of the size of the area scanned. Nominal magnifications indicated

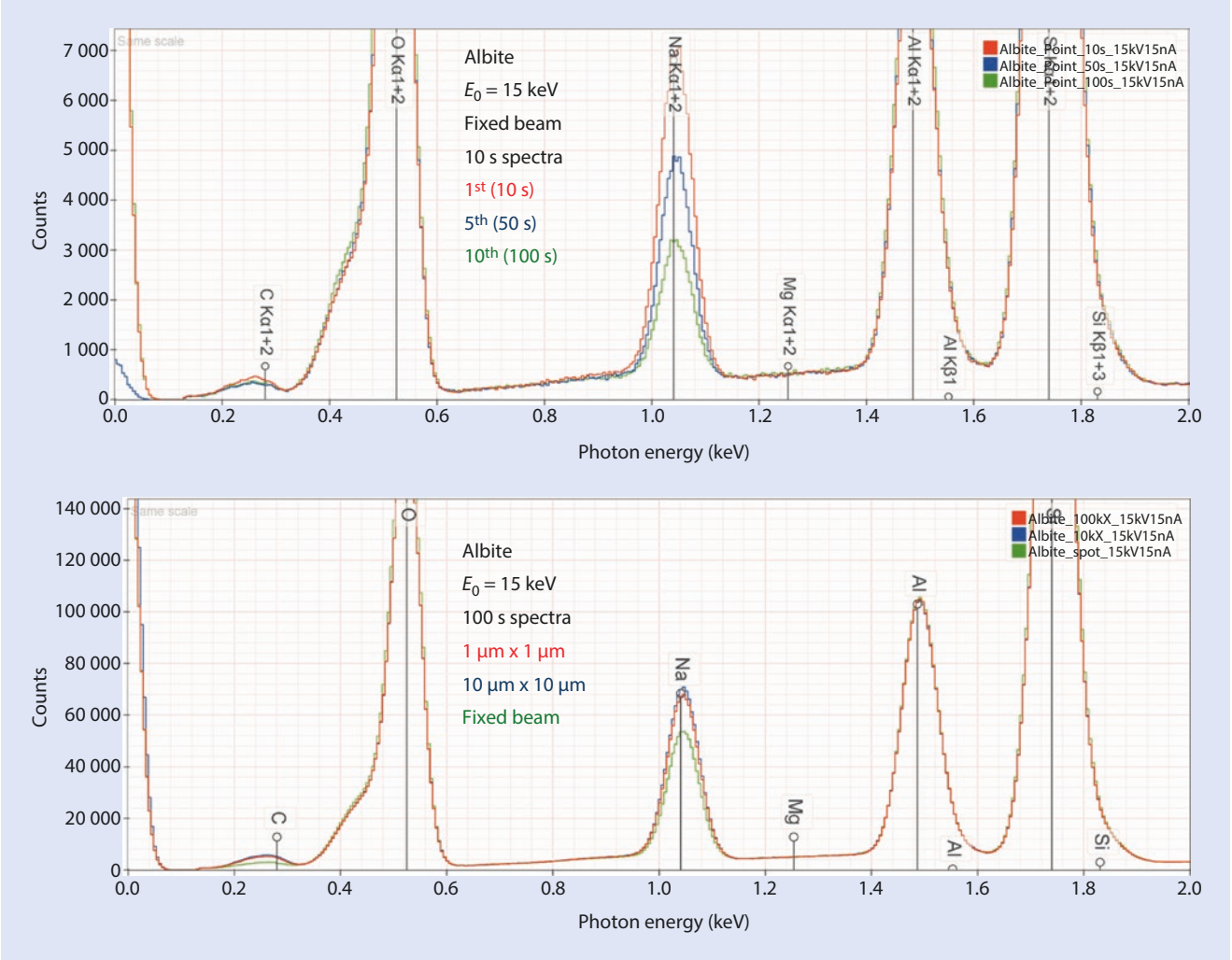

Fig. 20.18 Albite ($NaAlSi_3O_8$); E_0 = 15 keV, 15 nA: (*upper*) effect of increasing dose on the Na peak; (*lower*) effect of fixed beam versus scanned beam on the Na peak

CO, CO_2, and H_2O that evaporate into the vacuum, causing substantial mass loss from the interaction volume. At the highest beam currents, typically 10–100 nA, used with a focused beam at a static location, it is also possible to cause highly damaging temperature elevations, which further exacerbate mass loss. Indeed, when analyzing this specimen class it should be assumed that significant mass loss will occur during the measurement at each point of the specimen. If all constituents were lost at the same rate, then simply normalizing the result would compensate for the mass loss that occurs during the accumulation of the X-ray spectrum. Unfortunately, the matrix constituents (principally carbon compounds and water) can be selectively lost, while the heavy elements of interest in biological microanalysis (e. g., Mg, P, S, K, Ca, Fe, etc.) remain in the bombarded region of the specimen and appear to be present at effectively higher concentration than existed in the original specimen. What is then required of any analytical procedure for biological and polymeric specimens is a mechanism to provide a meaningful analysis under these conditions of a specimen that undergoes continuous change.

Marshall and Hall (1966) and Hall (1968) made the original suggestion that the X-ray continuum could serve as an internal standard to monitor specimen changes. This assumption permitted development of the key procedure for beam-sensitive specimens that is used extensively in the biological community and that is also applicable in many types of polymer analysis. This application marks the earliest use of the X-ray continuum as a tool (rather than simply a hindrance) for analysis, and that work forms the basis for the development of the peak-to-local background method applied to challenging geometric forms such as particles and rough surfaces. The technique was initially developed for applications in the high beam current EPMA, but the procedure works well in the SEM environment.

The Marshall–Hall method (Marshall and Hall 1966) requires that several key conditions:

1. The specimen must be in the form of a thin section, where the condition of "thin" is satisfied when the incident beam penetrates with negligible energy loss. For an analytical beam energy of 10–30 keV, the energy loss

passing through a section consisting of carbon approximately 100–200 nm in thickness will be less than 500 eV. This condition permits the beam energy to be treated as a constant, which is critical for the development of the correction formula. Biological specimens are thus usually analyzed in the form of thin sections cut to approximately 100-nm thickness by microtome. Polymers may also be analyzed when similarly prepared as thin sections by microtoming or by ion beam milling. Such a specimen configuration also has a distinct advantage for improving the spatial resolution of the analysis compared to a bulk specimen. The analytical volume in such thin specimens is approximately the cylinder defined by the incident beam diameter and the section thickness, which is at least a factor of 10–100 smaller in linear dimensions than the equivalent bulk specimen case at the same energy, as shown in the polymer etching experiment in the Interaction Volume module.

2. The matrix composition must be dominated by light elements, for example, C, H, N, O, whose contributions will form nearly all of the X-ray continuum and whose concentrations are reasonably well known for the specimen. Elements of analytical interest such as Mg, P, S, Cl, K, Ca, and so on, the concentrations of which are unknown in the specimen, must only be present preferably as trace constituents (<0.01 mass fraction) so that their effect on the X-ray continuum can be neglected. When the concentration rises above the low end of the minor constituent range (e.g., 0.01 to 0.05 mass fraction or more), the analyte contribution to the continuum can no longer be ignored.
3. A standard must be available with a known concentration of the trace/minor analyte of interest and for which the complete composition of low-atomic-number elements is also known and which is stable under electron beam bombardment. Glasses synthesized with low atomic number oxides such as boron oxide are suitable for this role. The closer the low–atomic-number element composition of the standard is to that of the unknown, the more accurate will be the results.

The detailed derivation yields the following general expression for the Marshall–Hall method:

$$\frac{I_{ch}}{I_{cm}} = c\frac{\dfrac{C_A}{A_A}}{\sum_i \left[C_i \left(\dfrac{Z_i^2}{A_i} \right) \log_e \left(1.166 \dfrac{E_0}{J_i} \right) \right]} \qquad (20.9)$$

In this equation, I_{ch} is the characteristic intensity of the peak of interest, for example, S K-$L_{2,3}$ or Ca K-$L_{2,3}$, and I_{cm} is the continuum intensity of a continuum window of width ΔE placed somewhere in the high energy portion of the spectrum, typically above 8 keV, so that absorption effects are negligible and only mass effects are important. C_i is the mass concentration, Z_i is the atomic number, and A_i is the atomic weight. The subscript "A" identifies a specific trace or minor analyte of interest (e.g., Mg, P, S, Cl, Ca, Fe, etc.) in the organic matrix, while the subscript "i" represents all elements in the electron-excited region. E_0 is the incident beam energy and J is the mean ionization energy, a function only of atomic number as used in the Bethe continuous energy loss equation

Assumption 2 provides that the quantity $\sum(C_i \cdot Z_i^2/A_i)$ in Eq. (20.9) for the biological or polymeric specimen to be analyzed is dominated by the low-Z constituents of the matrix. (Some representative values of $\sum(C_i \cdot Z_i^2/A_i)$ are 3.67 (water), 3.01 (nylon), 3.08 (polycarbonate) and 3.28 (protein with S). Typically the range is between 2.8 and 3.8 for most biological and many polymeric materials.) The unknown contribution of the analyte, C_A, to the sum may be neglected when considering the specimen because C_A is low when the analytes are trace constituents.

To perform a quantitative analysis, Eq. (20.9) is used in the following manner: A standard for which all elemental concentrations are known and which contains the analyte(s) of interest "A" is prepared as a thin cross section (satisfying assumption 3). This standard is measured under defined beam and spectrometer parameters to yield a characteristic-to-continuum ratio, I_A/I_{cm}. This measured ratio I_A/I_{cm} is set equal to the right side of Eq. (20.9). Since the target being irradiated is a reference standard, the atomic numbers Z_i, atomic weights A_i and weight fractions C_i are known for all constituents, and the J_i values can be calculated as needed. The only unknown term is then the constant "c" in Eq. (20.9), which can now be determined by dividing the measured intensity ratio, I_A/I_{cm}, by the calculated term. Next, under the same measurement conditions, the characteristic "A" intensity and the continuum intensity at the chosen energy are determined for the specimen location(s). Providing that the low-Z elements that form the matrix of the specimen are similar to the standard, or in the optimum case these concentrations are actually known for the specimen (or can be estimated from other information about the actual, localized, material being irradiated by the electrons, and not some bulk property), then this value of "c" determined from the standard can be used to calculate the weight fraction of the analyte, C_A, for the specimen.

This basic theme can be extended and several analytes—"A," "B," "C," etc.—can be analyzed simultaneously if a suitable standard or suite of standards containing the analytes is available. The method can be extended to higher concentrations, but the details of this extension are beyond the scope of this book; a full description and derivation can be found in Kitazawa et al. (1983). Commercial computer X-ray analyzer systems may have the Marshall–Hall procedure included in their suite of analysis tools. The Marshall–Hall procedure works well for thin specimens in the "conventional" analytical energy regime ($E_0 \geq 10$ keV) of the SEM. The method will not work for specimens where the average atomic number is expected to vary significantly from one analysis point to another, or relative to that of the standard. A bulk specimen where the beam-damaged region is not constrained by the

dimensions of the thin section, so that the region continues to change during electron bombardment also violates the fundamental assumptions. Consequently, many materials science applications for "soft" materials cannot be accommodated by the classic Marshall–Hall procedure.

Bulk Biological and Organic Specimens

The quantitative procedures devised by Statham and Pawley (1978) and Small et al. (1979) for the analysis of particles and rough specimens have been adapted to the analysis of bulk biological and organic samples (Roomans 1981, 1988; Echlin 1998). The method is based on the use of the ratio between the intensity of the characteristic and background X-rays defined as P/B, where P and B are measured over the range of energies that defines an EDS peak. The rationale behind the development of the method is that since the characteristic and background X-rays are generated within nearly the same depth distribution, they are subject to the same compositional related absorption and atomic number effects. It is assumed that the percentage of characteristic X-rays absorbed by the sample is the same as the percentage of continuum X-rays of the same energy which are absorbed. In the ratio P/B, the absorption factor (A) is no longer relevant as it has the same value in the numerator as the denominator and thus cancels. Since backscattered electrons are being lost due to changes in atomic number (Z), there is a similar decrease in the efficiency of production of both peak and background. Because the reduced X-ray production affects both peak and background in a similar (although not identical way), this factor is also cancelled out to a first order when the ratio P/B is measured. Additionally, because nearly all biological and/or organic materials consist of low atomic number matrix elements ($Z_{max} = 10$) the secondary fluorescence effect (F) is low and can be treated as a secondary order correction.

Strictly, these assumptions only hold true for homogeneous samples as the characteristic and background X-rays will vary with changes in the average atomic number of the sample. However, this is not considered to have any significant effect in cases where the P/B ratio method is applied to fully hydrated specimens which contain 85–90 % water or to dried organic material containing a small amount of light element salts. The ratio of peak area to the background immediately beneath the peak is relatively insensitive to small changes in surface geometry. However, the sample surface should be as smooth as is practicable because uneven fracture faces give unreliable X-ray data because of preferential masking and absorption.

Spectra are processed by the following procedure. The peaks in the spectra of the unknown and a standard of similar composition are fit by an appropriate procedure, such as multiple linear least squares, to determine the peak area for element i, P_i. The spectrum after peak-fitting and subtraction is then examined again to determine the background intensity remaining in the peak region of interest, giving the corresponding B_i at the same photon energy. Once accurate P/B ratios are obtained, they can be used for quantitation in a number of ways. The P/B value for one element can be compared with the P/B value for another element in the same sample and to a first order:

$$\left(C_i / C_j\right) = h_{ij}\left[\left(P/B\right)_i / \left(P/B\right)_j\right] \tag{20.10}$$

where C_i and C_j are the percentage concentrations of elements i and j and h_{ij} is a correction factor which can be obtained from measurements on a standard(s) of known composition very similar in composition to the unknown. Once h_{ij} has been empirically for the element(s) of interest, measurements of the P/B ratio(s) from the unknown can be immediately converted into concentration ratios. An advantage of taking the double ratio of (P/B) in Eq. (20.10) is the suppression of matrix effects, to a first order.

Alternatively, the P/B value for an element in the sample can be compared with the P/B value for the same element in a standard provided there is no significant difference in the matrix composition between sample and standard. If the mean atomic number of a given sample is always the same, the Kramers' relationship shows that the background radiation is proportional to atomic number. If the mean atomic number of the sample is always the same, then

$$C_i = h_i\left(P/B\right)_i \tag{20.11}$$

where h_i is a constant for each element. If it is possible to analyze all the elements and calculate the concentration of elements such as C, H, O, and N by stoichiometry, then relative concentrations can be readily converted to absolute concentrations.

If there is a significant change in the composition between the unknown and standard(s), then a correction must be applied based upon the dependence of the continuum upon atomic number, following the original Marshall–Hall thin section method:

$$\left(C_i / C_j\right) = h_{ij}\left[\left(P/B\right)_i / \left(P/B\right)_j\right]\left[\left(Z_i^2 / A_i\right) / \left(Z_j^2 / A_j\right)\right] \tag{20.12}$$

where Z and A are the atomic number and weight.

The peak-to-background ratio method has been found to be as efficient and accurate for biological materials as the more commonly used ZAF algorithms, which have been designed primarily for analyzing non-biological bulk samples. Echlin (1998) gives details of the accuracy and precision of the method as applied to hydrated and organic samples. For the analysis of a frozen hydrated tea leaf standard where independent analysis by atomic absorption spectroscopy was available for comparison, peak-to-background corrections generally gave results within ±10 % relative for trace Mg, Al, Si, and Ca over a range of beam energies from 5 to 20 keV.

References

Echlin P (1998) Low-voltage energy-dispersive X-ray microanalysis of bulk biological specimens. Microsc Microanal 4:577

Hall T (1968) "Some aspects of the microprobe analysis of biological specimens" in Quantitative Electron Probe Microanalysis, ed. Heinrich K. (U.S. Government Printing Office, Washington, DC) 269

Kitazawa T, Shuman H, Somlyo A (1983) Quantitative electron probe analysis: problems and solutions. Ultramicroscopy 11:251

Lifshin E, Doganaksoy N, Sirois J, Gauvin R (1999) Statistical considerations in microanalysis by energy-dispersive spectrometry. Microsc Microanal 4:598

Marshall D, Hall T (1966) "A method for the microanalysis of thin films", in X-ray Optics and Microanalysis, eds. Castaing R, Deschamps P, Philibert J. (Hermann, Paris) 374

Newbury D, Ritchie N (2015a) Review: performing elemental microanalysis with high accuracy and high precision by Scanning Electron Microscopy/Silicon Drift Detector Energy Dispersive X-ray Spectrometry (SEM/SDD-EDS). J Mats Sci 50:493

Newbury D, Ritchie N (2015b) Quantitative electron-excited X-ray microanalysis of Borides, Carbides, Nitrides, Oxides, and Fluorides with Scanning Electron Microscopy/Silicon Drift Detector Energy-Dispersive Spectrometry (SEM/SDD-EDS) and NIST DTSA-II. Microsc Microanal 21:1327

Ritchie N, Newbury D, Davis J (2012) EDS Measurements at WDS precision and accuracy using a silicon drift detector. Microsc Microanal 18:892

Ritchie N, Newbury D (2012) Uncertainty estimates for electron probe X-ray microanalysis measurements. Anal Chem 84:9956

Roomans GM (1981) Quantitative electron probe X-ray microanalysis of biological bulk specimens. SEM/1981/II (AMF O'Hare, IL, SEM, Inc.,) p 345

Roomans GM (1988) Quantitative X-ray microanalysis of biological specimens. J Electron Microsc Tech 9:19

Small J, Heinrich K, Newbury D, Myklebust R (1979) Progress in the development of the peak-to-background method for the quantitative analysis of single particles with the electron probe. SEM/1979/II, p 807

Statham P, Pawley J (1978) A new method for particle X-ray microanalysis based on peak-to-background measurements. SEM/1978/I, p 469

Vicenzi E, Eggins S, Logan A, Wysoczanski R (2002) Microbeam characterization of Corning archeological reference glasses: new additions to the Smithsonian microbeam standard collection. J Res National Inst Stand Technol 107:719

Ziebold T (1967) Precision and sensitivity in electron microprobe analysis. Anal Chem 39:858

Ziebold T, Ogilvie R (1964) An empirical method for electron microanalysis. Anal Chem 36:322